Chapter 5

Data Analysis for RUL Estimation

5.1 Introduction

The present study contributes to the selection of a prognostic parameter for assessment of the life of motors in AMT automobiles. Having observed the unusual patterns in the sensor dataset collected from the experiment, current (I_a) signal as one such prognostic parameter is proposed to exhibit the state of the health of the clutch. A novel condition indicator and threshold for the conditionally independent noisy current signal of the motor subjected to cumulative degradation have also been established to forecast the RUL. Predictive maintenance utilizes three well known data-driven methodologies for estimating the RUL, namely the lifetime data from similar machines, run-to-failure data and threshold approach. In the subsequent sections, visualization to the ALCT experimental dataset for three different strategies along with their preprocessing results will be elaborated. The feature fused CI for each of the three different experimental strategies needs to be finalized. The scatter plot of the selected indicator will provide a clue regarding the determination of the threshold (López de Calle et al. 2019) for RUL estimation. The RUL estimation findings for a data-driven study using the proposed CI, together with the results of degradation data modelling utilizing exponential degradation approach and particle filtering method, can aid in anticipating early failures of the *e*-AMT clutch.

5.2 Experimental Details

The ALCT test has been the proposed strategy for the data collection. The clutch provides a transfer of rotating torque from one shaft to the other. Under the adequate operation, the clutch permits gradual loading. For an AMT automobile, the motor is pushed to work beyond the permissible limits in actual driving condition, which may results in an unexpected failure prior to the given service lifetime (Fagang et al. 2009; Liu et al. 2017; Suh et al. 1999; Saravanan and Altaf 2014; Saidi et al. 2017). Three different accelerated loading strategies are motivated with the change in duty cycle parameter. The two phenomenon i.e., engagement and dis-engagement guides the clutch operations by taking a duty cycle input. In order to attain system reliability, three optimal strategies are designed by varying the duty cycle load.

Estimation of system reliability for a rotating machinery with untested components was seen to be conducted with the application of sequential-ALCT (Hu and Mourelatos 2018). For an

automotive system, the ALCT also implies a smaller amount of time that will be required for testing, to meet the design criterion. The PMDC motor assists the electromechanical actuator in an *e*-AMT clutch actuation. The motor responds at 0.5milli-sec while the feedback current (I_a) was captured at 10milli-sec interval to the micro-controller. This time interval is found to be long enough to damage the motor control unit. Proposed methodology in Fig. 4.2 of chapter 4 involves using one of the data driven approaches, (namely the exponential degradation model) (Coble 2010; Jouin et al. 2016; Lei et al. 2018; Zhu et al. 2020) for meaningful interpretation of the changes in this period of transient operation. The motor current has been found to possess dynamic fluctuating nature. The inability to capture such transients and its effects on the motor life provides a scope to the present study. The next section 5.2.1 provides a brief overview to the three in-vitro developed ALCT strategies. However, illustration of a dynamic waveform for a sample data has been presented in the subsequent sections.

5.2.1 Waveforms of the Accelerated Life Cycle Test Data

The present work makes use of the three different ALCT strategies for generating experimental data. “Strategy 1” uses 50% duty cycle for clutch engagement and a 70% duty cycle for clutch dis-engagement. “Strategy 2” uses 75% duty cycle for clutch engagement and an 80% duty cycle for clutch dis-engagement whereas, during “Strategy 3” an 80% duty cycle was used for clutch engagement whereas an 85% duty cycle for clutch dis-engagement. A relatively increasing range of duty cycles affirms the faster motor response timings by 22 percent in strategy–II and up to 30 percent in strategy-III while undergoing harsh operating conditions. The decrease in current value had been observed with the increase in duty cycle loading. This may be due to the faster rate of response to accommodate the gear shifting. The During an uphill condition a clutch encounters a clutch-biting point where, the gravity force is balanced by the static friction of the wheels. For a passenger car to move under such conditions, a higher acceleration is required which in turn demands higher duty cycle load. The following work features three different driving conditions during a city drive cycle. The data were logged using the sensors (list of all the sensors can be found in Table 3.1) and the INCA software by ETAS module helped in storage of the data in ASCII and DAT format.

This raw data is to be then used for feature extraction, which is further used for training the empirical motor model for motor prognostics. The three sub-sections of 5.2.1 consists of sample waveforms for the three experimental strategies.

5.2.1.1 Strategy I: (50%-70%)

ALCT data have been collected in order to test the endurance of the PMDC motor. Figs 5.1-5.7 corresponds sample plots to the first set of experiments conducted on the HIL. The clutch movement offered the initial choice of the 50percent duty for engagement and 70percent for disengagement while the variation of the current data was closely observed.

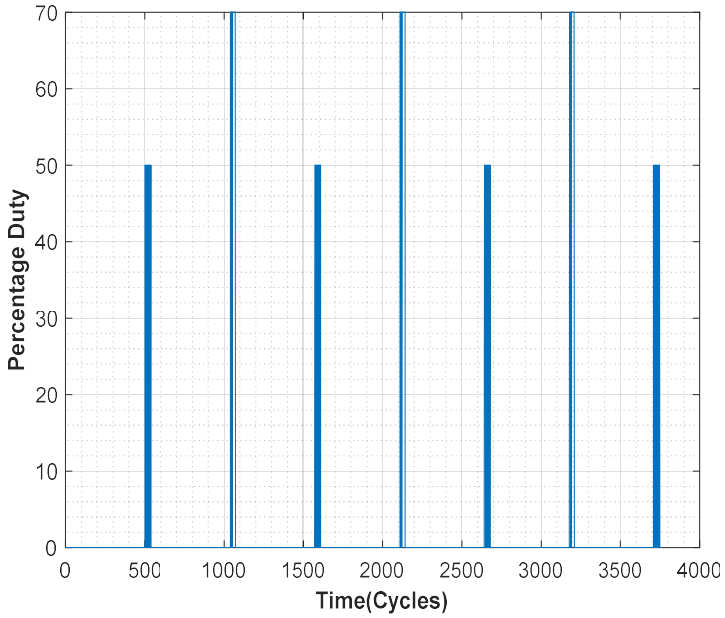

Figure 5.1 Sample representation of a 50% -70% duty cycle input to the motor

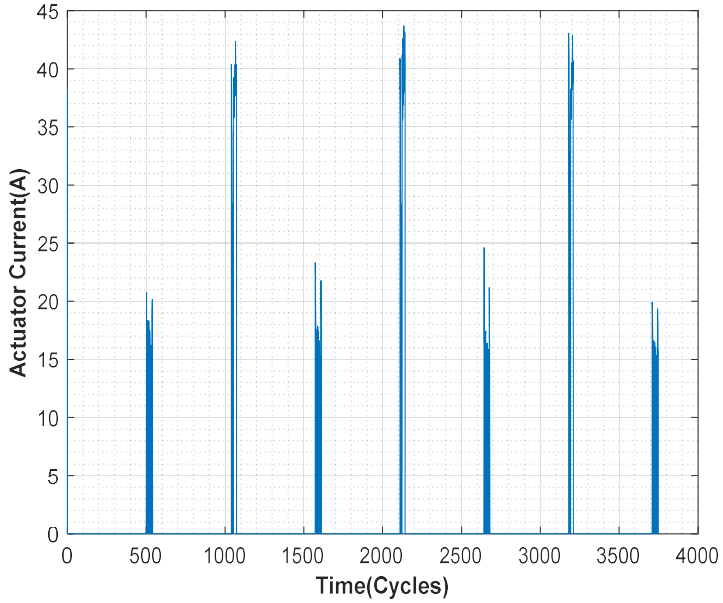

Figure 5.2 Sample representation of motor current response for 50% -70% duty cycle

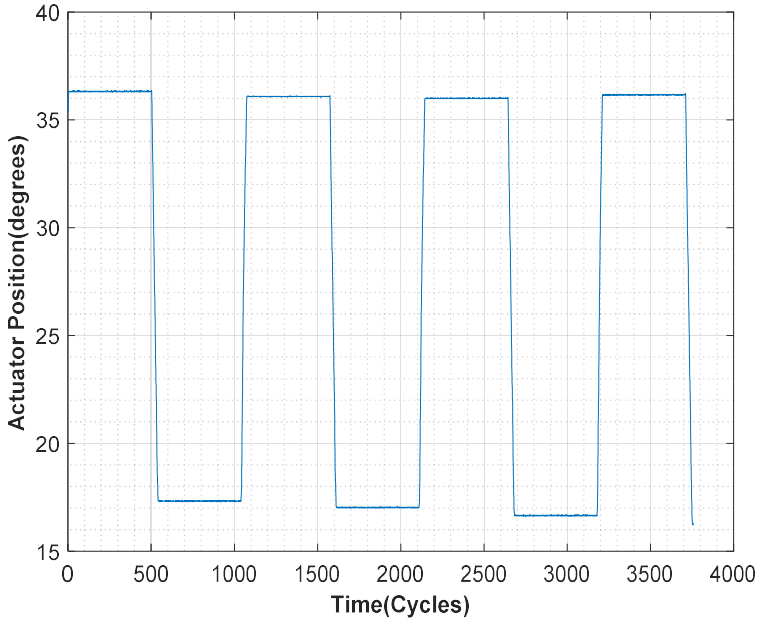

Figure 5.3 Sample plot of actuator position (degrees) during 50% -70% duty cycle

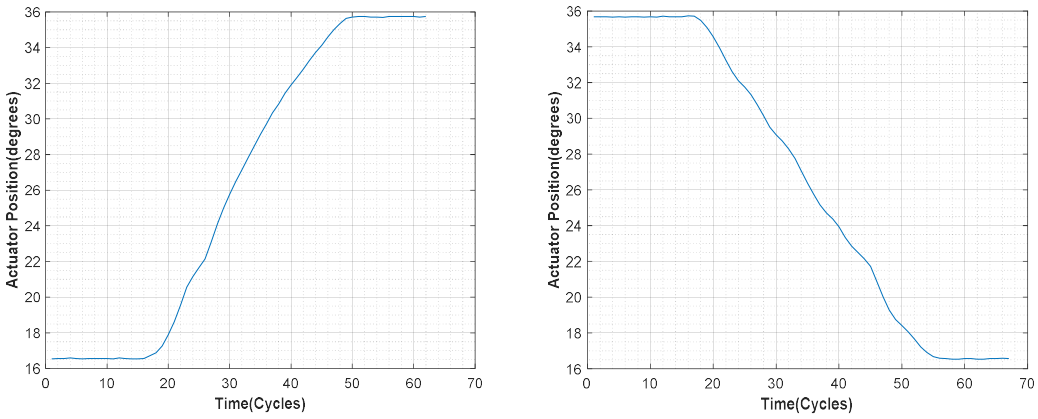

Figure 5.4 Magnified sample plot representing clutch (a) Disengagement, and (b) Engagement

The Fig. 5.3 illustrates a sample plot of the clutch engagement-disengagement for three cycles. The clutch actuator position for disengagement (approximately from 16 to 36degree) and the subsequent reversal is the engagement cycle represented in Fig. 5.4(a, b). The sample plot in Fig. 5.5 and 5.6 illustrates all the three sensor variables used during data collection during experimentation for life prediction of the clutch motor setup until failure.

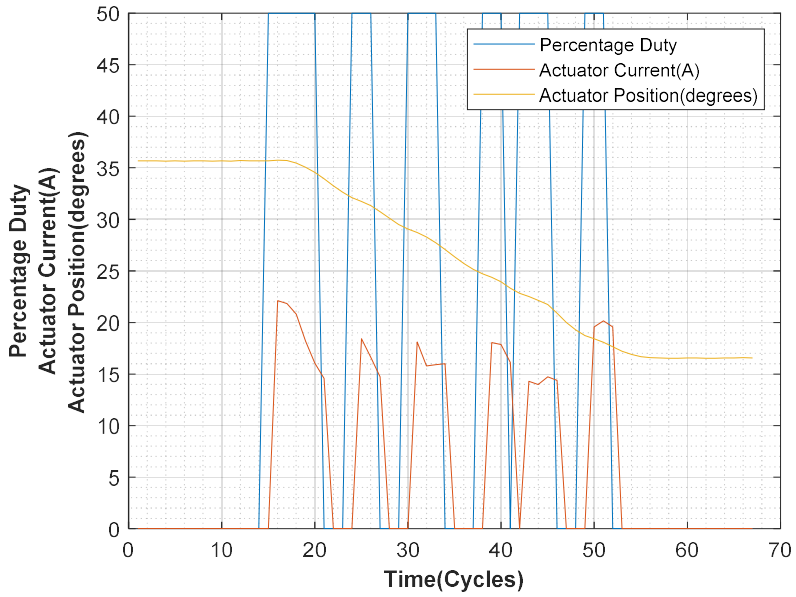

Figure 5.5 Variation of duty, current and actuator position for a sample clutch engagement cycle

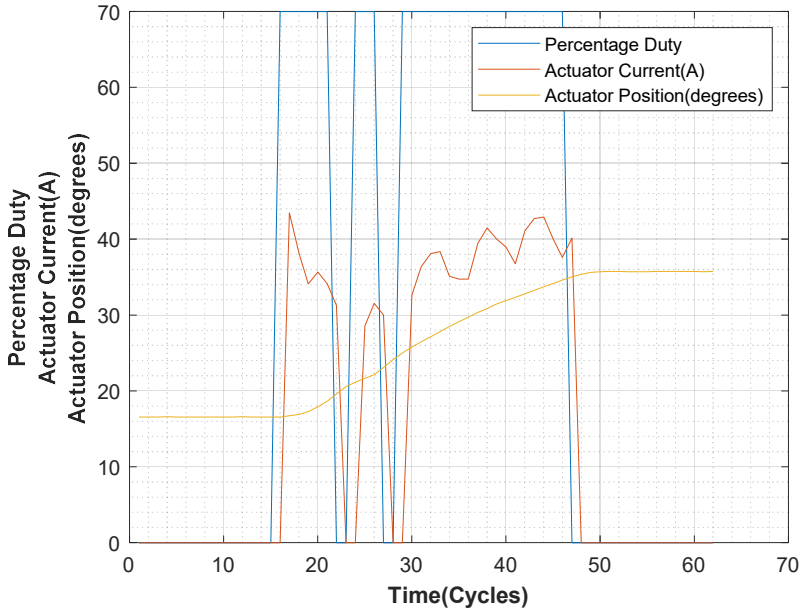

Figure 5.6 Variation of duty, current and actuator position for a sample clutch dis-engagement cycle

5.2.1.2 Strategy II: (75%-80%)

The second set of ALCT experiments were performed under similar conditions of continuous voltage power supply (recorded value of 14 volts) and increased loading conditions (see Fig. 5.7). For clutch actuation, a duty cycle value of 80percent for disengagement and 75percent for engagement. The movement in actuator position had been observed to occur from 16-33degrees

and vice-versa during reciprocation cycles with faster rate of response. After each complete cycle, a 5seconds dwell period was observed. The present day computer controlled cars necessitates the dwell time which contrasts to an appreciable amount of time in order to build up the maximum RPM for further reciprocation. The clutch usually remains in an engaged state, therefore it requires an initial higher duty cycle to disengage and fulfil the shifting of gears.

Fig. 5.7-5.10(a, b) below provides an illustration of the sample plots into the experimental background and the actual realizations.

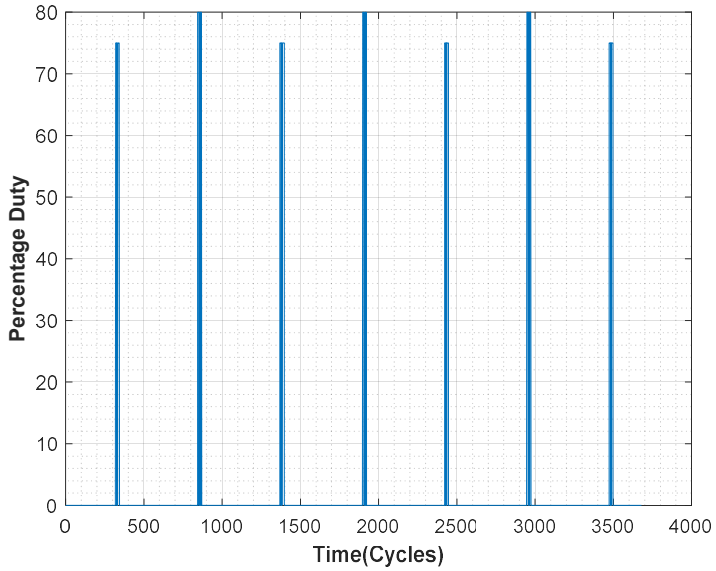

Figure 5.7 Sample representation of a 75% -80% duty cycle input to the motor

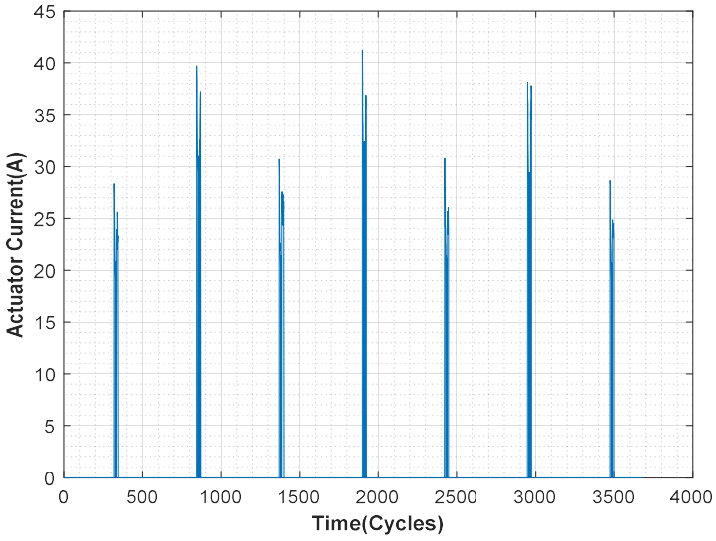

Figure 5.8 Sample representation of motor current response for 75% -80% duty cycle

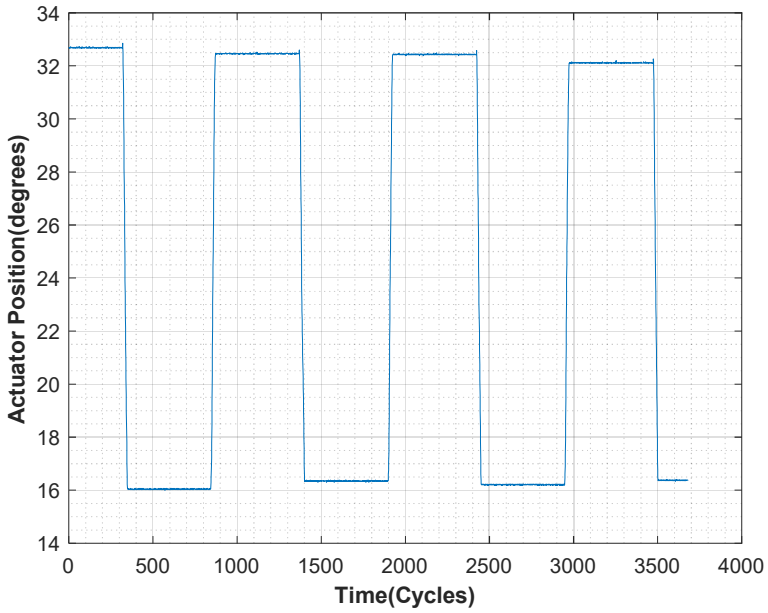

Figure 5.9 Sample plot of actuator position (degrees) during 75% -80% duty cycle

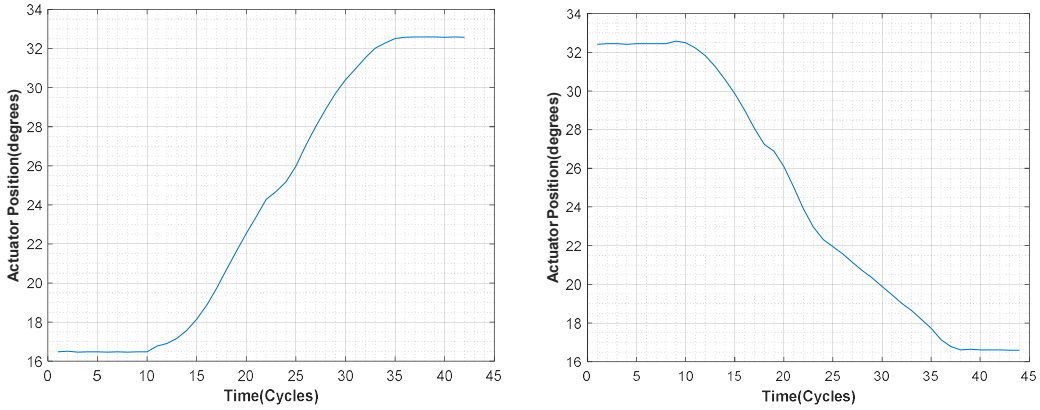

Figure 5.10 Magnified sample plot representing clutch (a) Disengagement, and (b) Engagement

Fig. 5.9 illustrates a sample plot of the clutch engagement-disengagement for three cycles. The movement from 16 to 33degree is clutch disengagement and it consumes 25ms while the subsequent reversal happens in approximately 29ms i.e., the engagement cycle, as represented in Fig. 5.10(a, b).

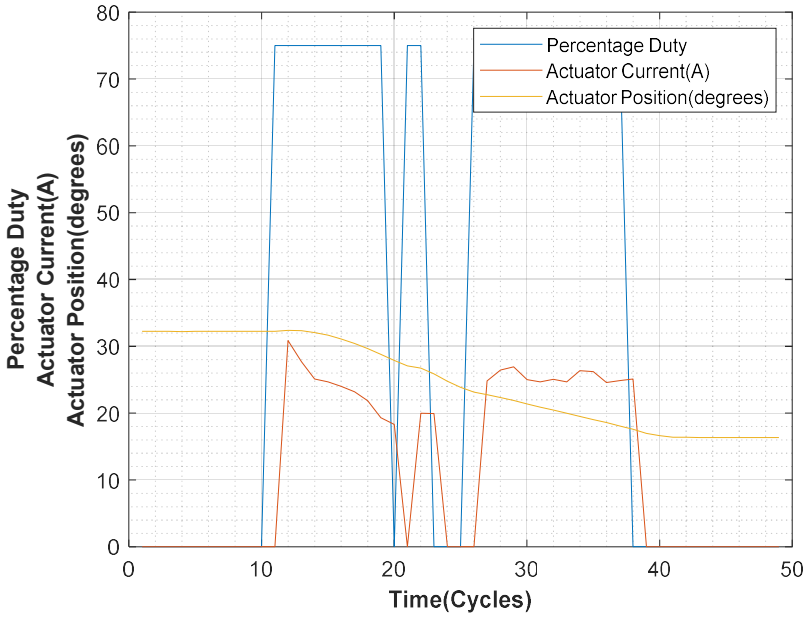

Figure 5.11 Variation of duty, current and actuator position for a sample clutch engagement cycle

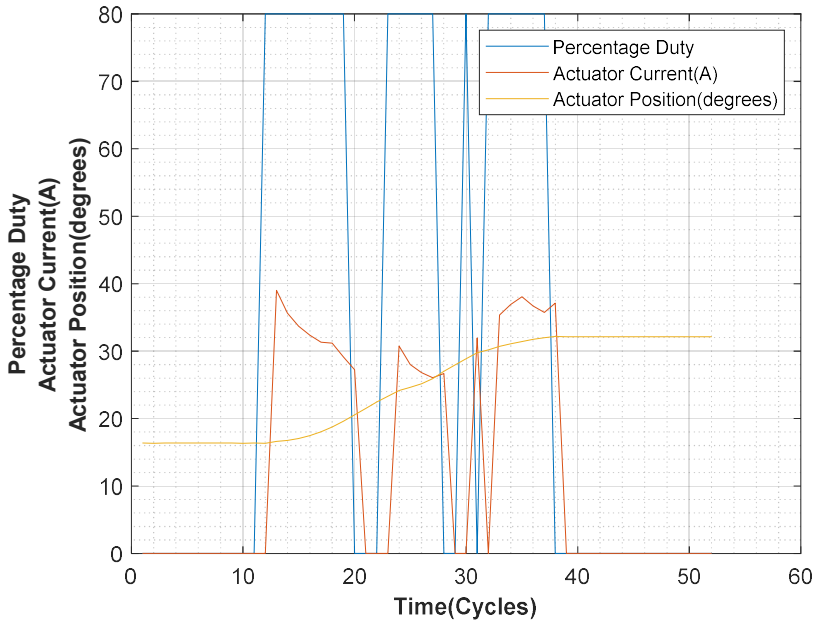

Figure 5.12 Variation of duty, current and actuator position for a sample clutch dis-engagement cycle

The sample plot in Figs. 5.11 and 5.12 narrates the three sensor variables data captured during experimentation for life prediction of the PMDC motor.

5.2.1.3 Strategy III: (80%-85%)

The continuously increasing magnitude of duty cycle (ranging from 80percent to 85percent) during the ALCT test was intended to generate faster actuation at full load conditions. The clutch actuation using electromechanical actuator readily consumes a fraction of a second for a single cycle operation. As stated earlier that the motor is operated at 0.5ms while the controller response being 10ms makes the job cumbersome. The cycle time for the clutch shifting thereby decreased to 10.04 seconds. For an *e*-AMT vehicle, the need for an electromechanical actuator with higher endurance becomes a must for the user under normal riding conditions in a city drive cycle.

In-vitro strategy-III has been designed keeping in mind a higher traffic conditions during an actual ride day where gear shifting increases drastically thereby disrupting the motor's normal working capacity beyond permissible limits. The normal operation being huge while the faulty data is insufficient which once again necessitates for varying needs of the PWM. In the process the current consumption provides an actual threat for the PMDC motor. It is the higher current that objectifies the need to the present study using CBM tool. Generation of higher current will in turn generate high heating of the clutch motor. The heating leads to a premature failure of the motor windings. However, a heavy loading might cause an early clutch lining failure also, besides decreasing the clutch life.

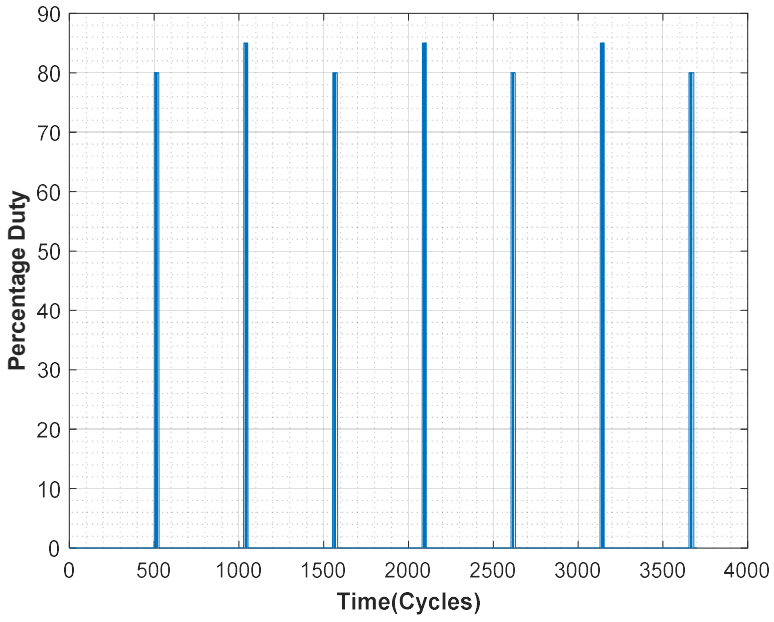

Figure 5.13 Sample representation of an 80% -85% duty cycle input to the motor

Experiments have been made to run till the actuator encounters failure. The presence of transient currents beyond permissible limit (51.926 Amps) at torque level resembles the onset of motor failure. The experimental data collected have been presented in Fig. 5.13-5.16(a, b). Visualizations for the two clutch positions are distinguishable in a separate picture to provide an idea of complete disengagement and engagement.

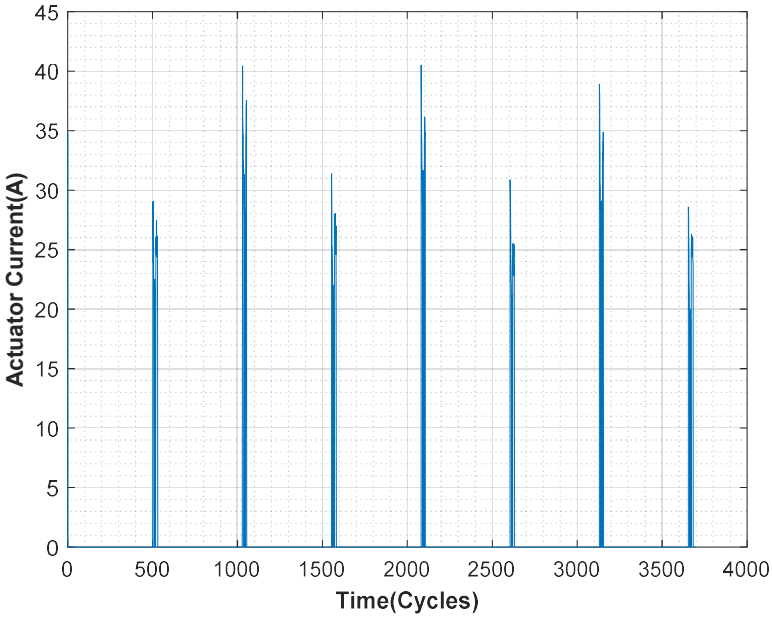

Figure 5.14 Sample representation of motor current response for 80% -85% duty cycle

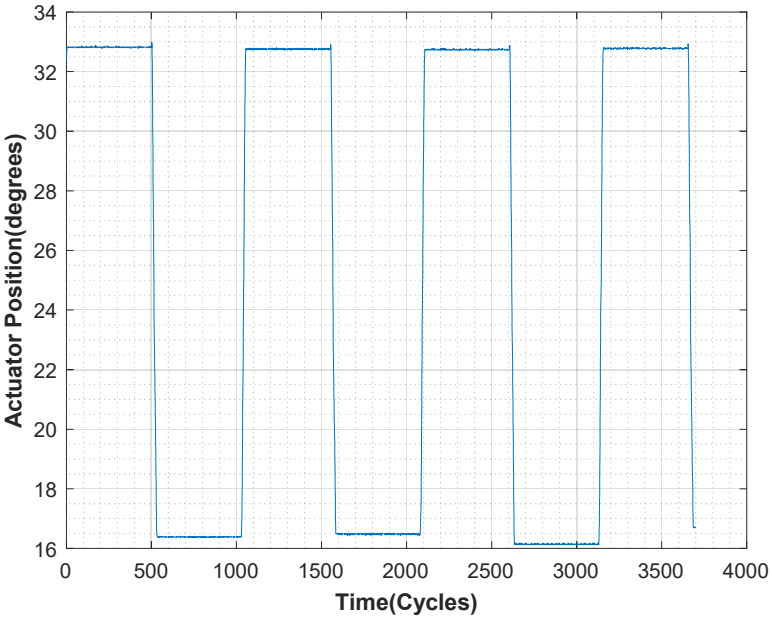

Figure 5.15 Sample plot of actuator position (degrees) during 80% -85% duty cycle

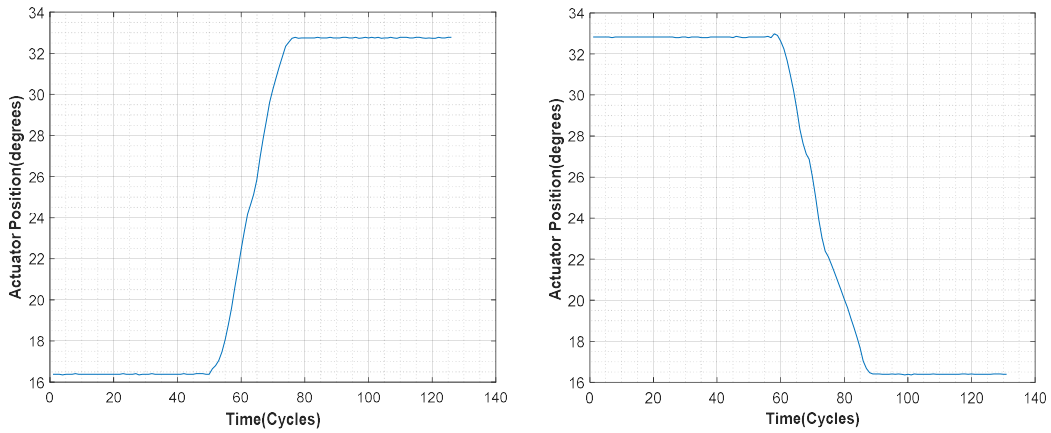

Figure 5.16 Magnified sample plot representing clutch (a) Disengagement, and (b) Engagement

The position from 33degree to 27degree is the partial disengagement while the actuators attaining to an exact position of 16 and 33degree is said to be complete disengaged or complete engaged. Length of one cycle has been calculated on the basis of complete engagement disengagement. Complete picture of all the monitored variables for Strategy III can be found from the Fig. 5.17 & 5.18.

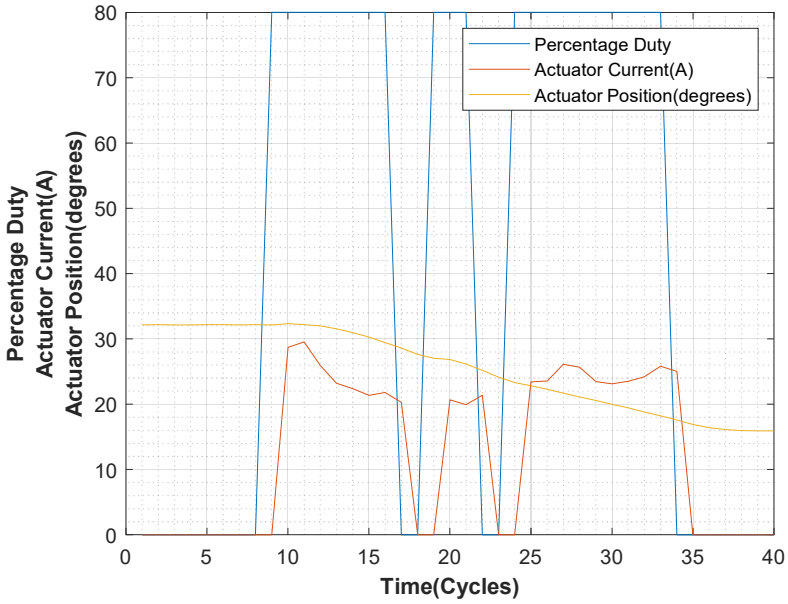

Figure 5.17 Variation of duty, current and actuator position for a sample clutch engagement cycle

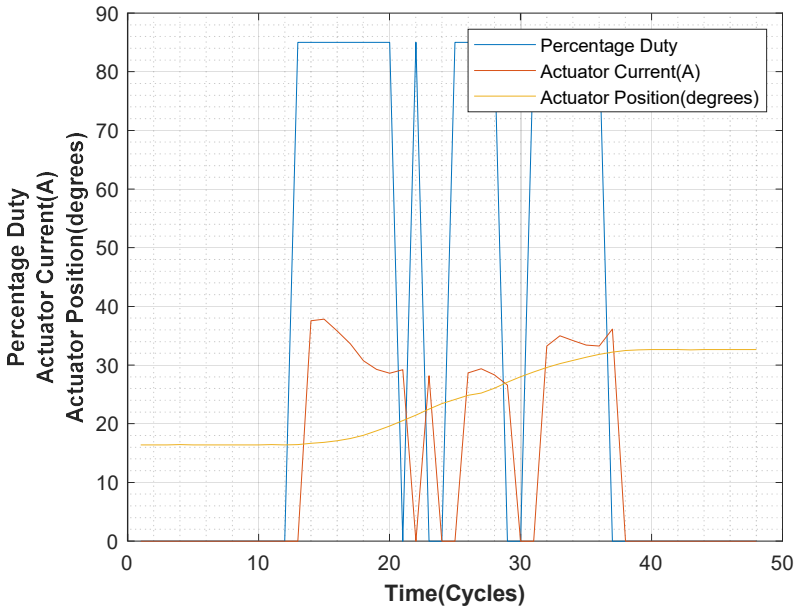

Figure 5.18 Variation of duty, current and actuator position for a sample clutch engagement cycle

5.3 Results and Discussion

5.3.1 Feature Extraction and Smoothing

The present work considers the degradation motor current (I_a) data out of all the monitored variables during experimentation for motor health prognosis. The three sets of motor degradation data are said to undergo the below mentioned machine learning schematic (see Fig. 5.19) for data pre-processing. The use of machine learning technique for data processing is an initial approach to the work. Motor prognostics cannot be directed using the raw values. The raw data consists of transients which are responsible for motor degradation and failure. From the actual dataset, statistical features are obtained which is followed by smoothening of the features (see Fig. 5.20 (a, b, c)). While development of the prognostic algorithm relies on huge amount of dataset, an initial 60percent of it is used for training. The choice of training data is reasonable as it captures the machines early life cycles behaviour. Feature importance step uses the normalized features, in order to plot the results in a same scale.

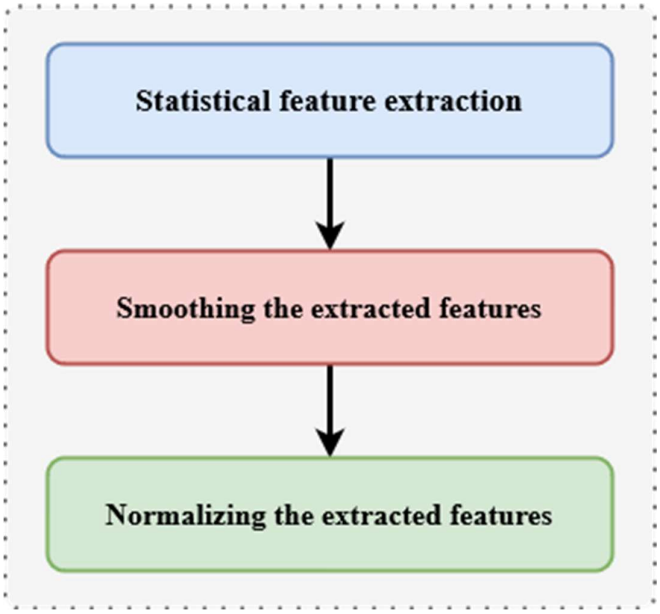

Figure 5.19 Steps of data pre-processing

The statistics of the signal is processed from the extracted features using the logged data in time domain, frequency domain and the time-frequency domain. Significant changes in statistical properties are observed for faulty conditions as compared to a normal operating regime in a machine. Better known time domain features help in categorizing the system's healthy state using increasing order of moments. The equations in Table 4.1 of Chapter 4 depict the respective features with symbols denoting their actual meanings. Additionally, frequency domain and time-frequency features are also introduced to better characterize the signals. The Strategy-I data consists of 319cycles, 249cycles is the length of Strategy-II and Strategy-III has 520cycles data.

The plots in Fig. 5.20 (a, b, c) represents the smoothened characteristic features of the current signal. For a real-time smoothening of data, moving average filter have been used to compensate the unavailability of future sample points. All the features from the three set of experimental strategies undergo data smoothening.

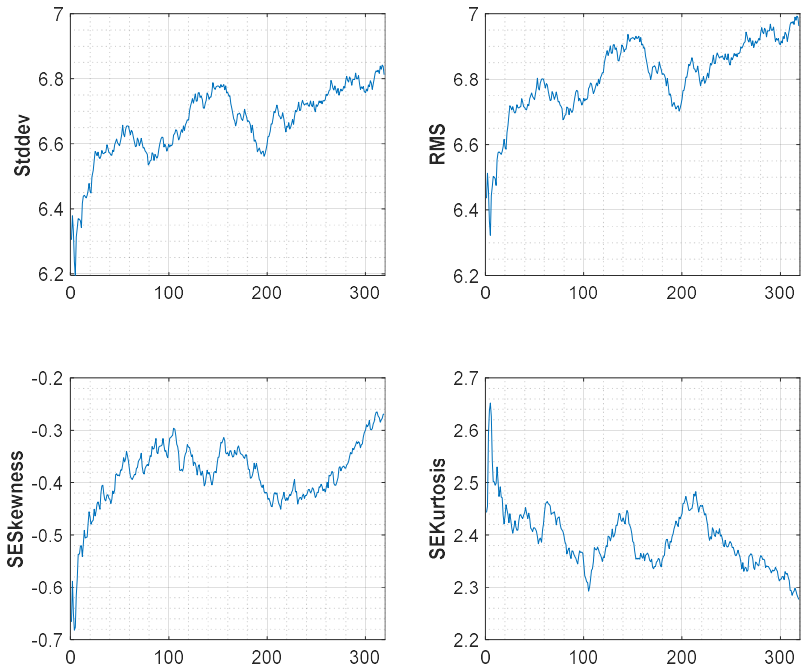

Figure 5.20 (a) Smoothened features of the sensor data using classical time domain, frequency domain and time-frequency domain methods Strategy-I

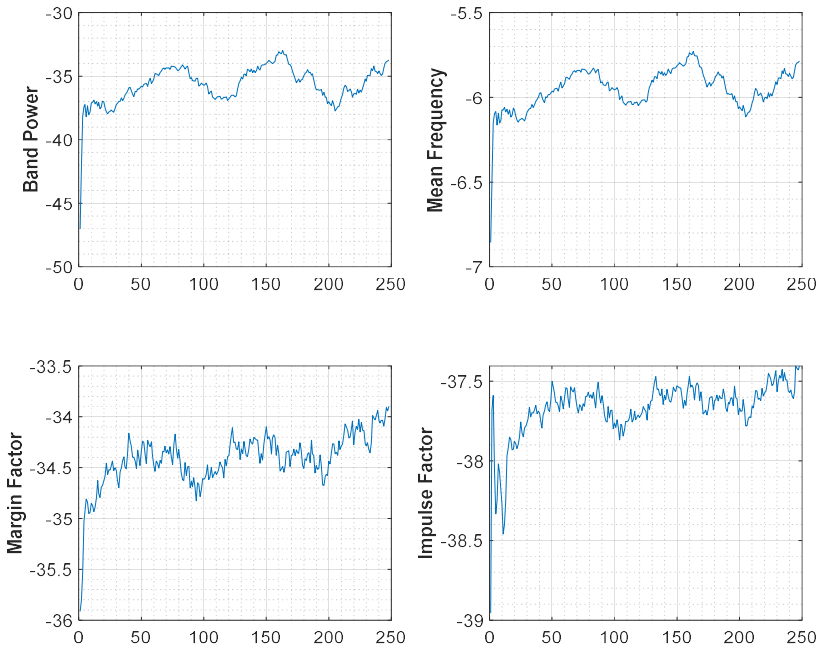

Figure 5.20 (b) Smoothened features of the sensor data using classical time domain, frequency domain and time-frequency domain methods Strategy-II

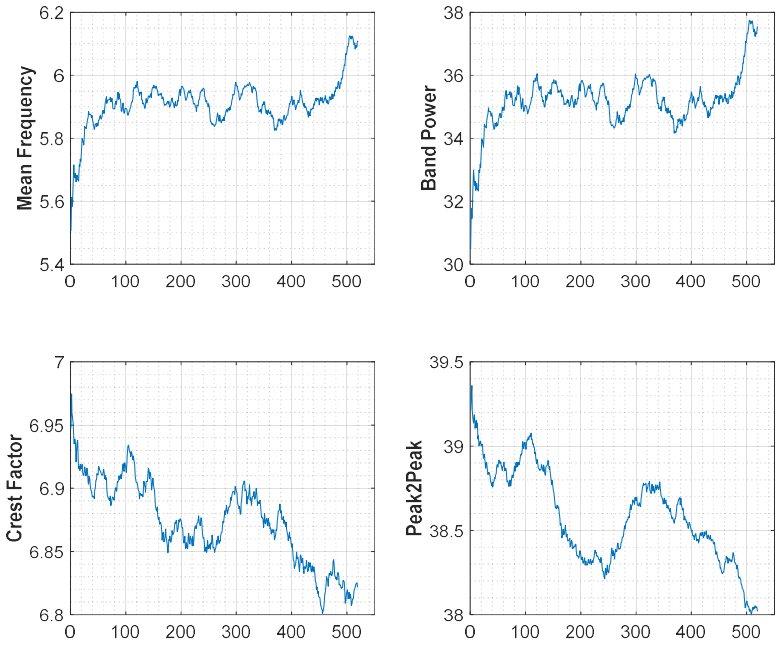

Figure 5.20 (c) Smoothened features of the sensor data using classical time domain, frequency domain and time-frequency domain methods Strategy-III

The selection of the order of moving average is done on the basis of global trend and local variations. The mean frequency estimates the mean normalized frequency of the power spectrum in terms of sample rate for a signal. Whereas, band power computes the average power in the input signal. The noisy features extracted can hinder the performance of RUL prediction.

The next section describes the FIR for a training data and the methodology in developing a novel CI. Importance ranking is linear function of the monotonocity and trendability metrics (refer Eq. (4.7)). Finally, by means of PCA based feature fusion the CI for all three strategies are developed.

5.3.2 FIR and Condition Indicator

The concept of minimum redundancy and maximum relevance is adapted to select best derived features for an unlabeled class of data by means of unsupervised feature selection technique. The prognostic metrics takes into account both the relevance and the redundancy between features via the mutual information criteria (Wang et al. 2017). Monotonocity (Coble 2010; Gomes et al. 2016; Liao 2014) and trendability (Coble and Wesley Hines 2009) metrics were used to rank the best, out of all the characteristic features. For selection of a good prognostic indicator, the metrics need to be consistent i.e., either increasing or constant but not decreasing.

The two proposed metrics were used to derive the fitness function (in Eq. (4.7)) for contributing the analogy in PCA fusion and ranking of the fused features. PCA is a feature extraction process that uses a dimensionality reduction technique by means of an orthogonal transformation. For an exploratory analysis of data, the principal components comprise of a decreasing order of variance. Section 4.2.4 discusses the PCA based feature fusion in details. The computed value using Eq. (4.7) for FIR gives a clear indication in selecting the appropriate CI as illustrated in Fig. 5.21(a, b, c).

The bars in each figure represents the most dominant characteristic for the condition monitored data along the decreasing order of magnitude (i.e., the higher magnitude ranks first). All the top ranked features resemble similar pattern in degradation characteristic of the motor that can be further seen in the Fig. 5.22 where all the three CI's are plotted.

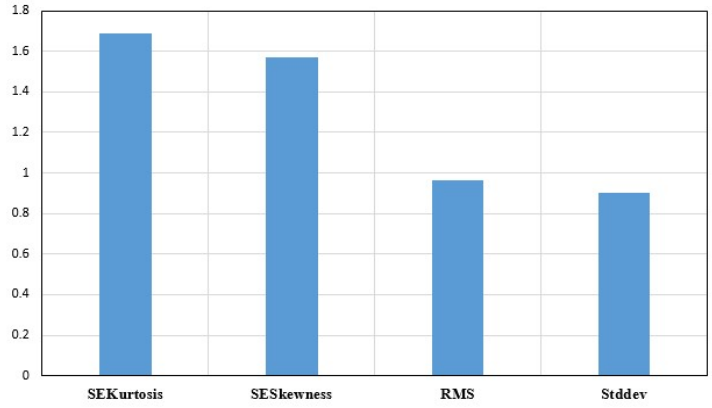

Figure 5.21 (a) Ranking of the important preprocessed features Strategy-I

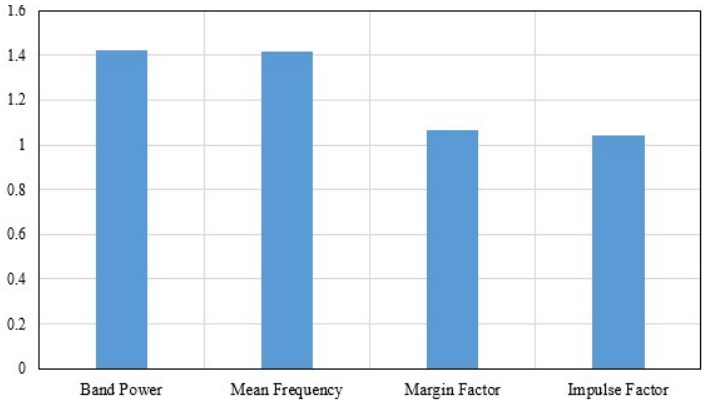

Figure 5.21 (b) Ranking of the important preprocessed features Strategy-II

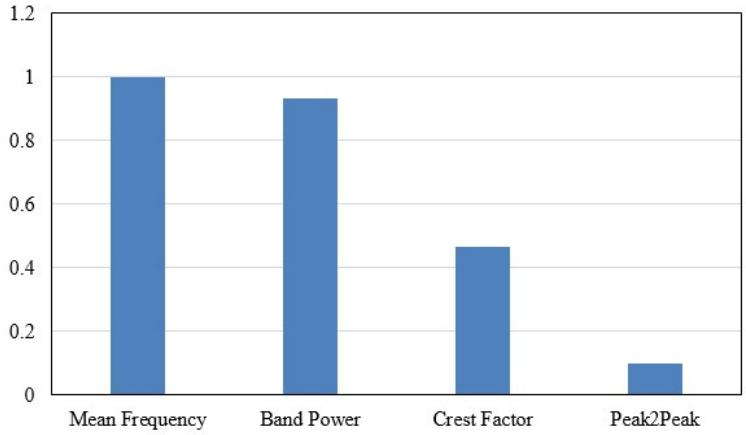

Figure 5.21 (c) Ranking of the important preprocessed features Strategy-III

CI is formulated using the top 60% of the ranked features from FIR. The use of Eigen vector for feature fusion further simplifies the selection of CI as is discussed in the Chapter 4. The use of Fisher's discriminant ratio (Lei et al. 2018) for best feature selection was seen in the works related to condition monitoring of cutting tools in an industry. The cutting force values at each operation were collected to find out the most relevant features within the time and frequency domain. Similarity amongst a few of them and a much higher difference between the features were found to be a good measure for the time-series data. Lei et al. (2018) categorizes construction of the health indicators into two types: physics based and virtual based health indicators. The former is extracted by means of statistical methods while the later used dimensionality reduction techniques a.k.a., fusion approach, to generate degradation trends in a rotating machinery. The dominance of PCA in the construction of virtual health indicators has been found in the application works of cutting tools (Benkedjouh et al. 2015), bearings (Wang et al. 2008), that helped us to feature the use of PCA in the construction of a CI. Suitability of our proposed CI for all the three datasets utilizes the metric depending on a single indicator with time. Monotonocity takes care of the irreversibility in the degradation phenomenon for a machinery i.e., no self-healing property and requiring human intervention during faulty state. The dependency of the motor with the number of operating hours, trendability has been used. Trendability correlates the degradation of the proposed feature with time. Both the metrics can be found mathematically expressed as under Eq. (4.5) and Eq. (4.6).

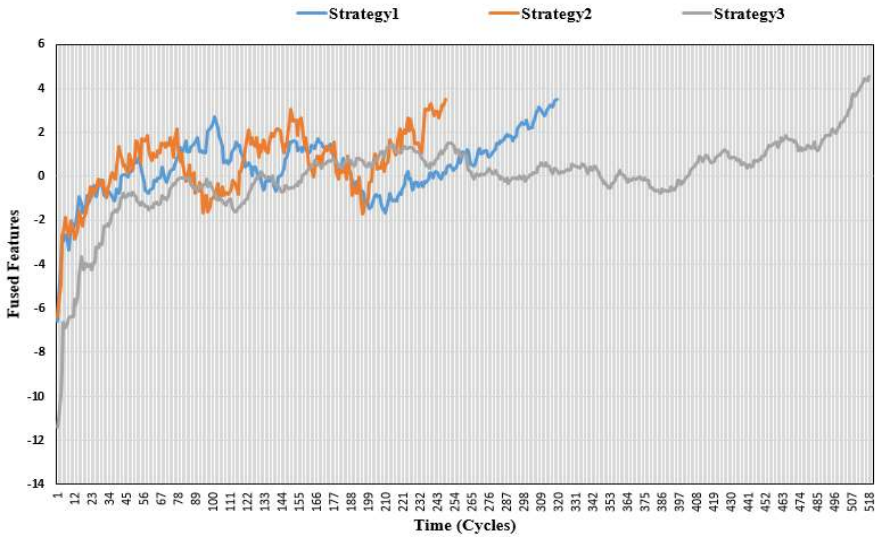

Figure 5.22 Condition indicators for all three strategies obtained after feature fusion

A novel CI matrix and the threshold (López de Calle et al. 2019) value were proposed out of the PCA fused feature. The developed CI's will be hereafter used for motor prognostics. The three CI's for the degradation motor dataset operating under three different duty cycle loading can be found plotted in Fig. 5.22. Note that even though the degradation rates for the motor under three different working conditions differ significantly, all the degradation motor signals exhibit similar characteristic trend. All the three CI's are upward monotonic and features an erratic fluctuation with the presence of noise. Challenge lies in handling the noise besides the RUL estimation via the two data-driven modeling techniques. The subsequent sections 5.3.3 and section 5.3.4 highlights the use of the developed CI for motor RUL prognostics. Section 5.3.5 elaborates the comparison results between the two prognostics methods used

5.3.3 Stochastic Approach

5.3.3.1 Exponential Degradation Model and RUL Computation

Degradation models (Celaya et al. 2012; Gebraeel 2006; Gebraeel et al. 2005; Liu et al. 2013; Wang et al. 2012; Zhou et al. 2011a) extrapolate past behavior of the degrading system to predict the future condition. They are used with a predefined safety threshold in the absence of run-to-failure data for similar machines under operation. The maximum value of the fused features was used as a threshold. These models are useful for a known value of the CI that indicates failure (Liu et al. 2013). The proposed approach uses an exponential degradation model for the PMDC motor that experiences cumulative degradation. A novel CI matrix and threshold value of the PCA fused feature were established and applied to the exponential degradation model. The PCA is a

dimensionality reduction approach which has been addressed in details in the earlier chapter 4. However, a random coefficients model (Gebraeel et al. 2009, 2005) was developed to link the real time data with the historical data. Bayesian updating criterion (see Fig. 5.23) for prediction and updating of parameters was carried out for estimation of RUL. Details of the distribution parameters have already been addressed in the previous chapter while explaining the model development strategy.

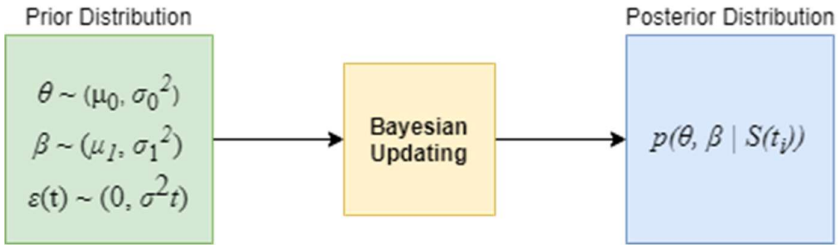

Figure 5.23 Bayesian updating of model parameters

Lu and Meeker (1993) introduced a modeling technique that updated the residual life using two conditions based error terms. Simulation results for all the three experimental strategies were evaluated for 500 runs and the use of prior parameter values for the exponential degradation model can be found summarized in the Table 5.1 below.

Table 5.1 Empirically fitted values of the exponential degradation model

	Dataset (Cycles)	**phi** (**Φ**)	**theta** (Θ)	**beta** (**β**)	**noise sdv.** (**σ**)	**threshold**
Strategy I	319	-3	0.2281	0.0044	0.1	3.5186
Strategy II	249	7	0.3703	0.0063	0.2	3.5056
Strategy III	520	-11.5	0.1091	0.0043	0.2	4.5184

However, Bayesian updating scheme was followed for updating the model parameters during each experimental run. The length of the dataset along with the threshold value and the initial parameter values are provided. The value of the noise standard deviation is assumed to cause a percentage of variation of the health indicator when it comes in the close periphery of the failure threshold. The prior values were finalized after 500 runs and value obtaining the lowest error were finalized.

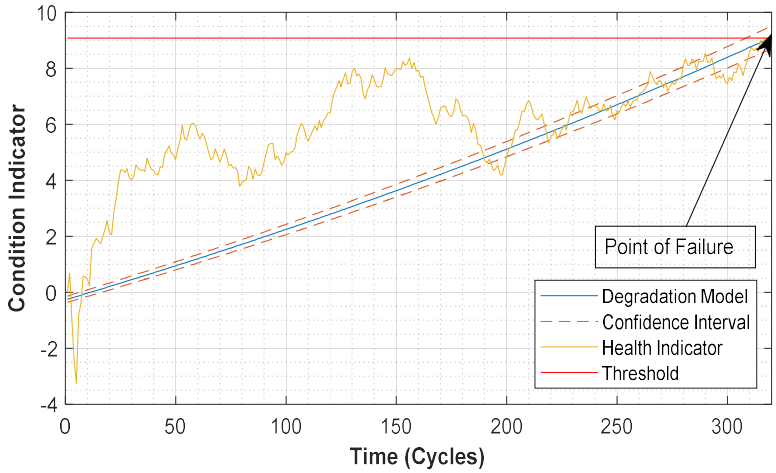

Figure 5.24 (a) Predicted RUL using exponential degradation model Strategy-I

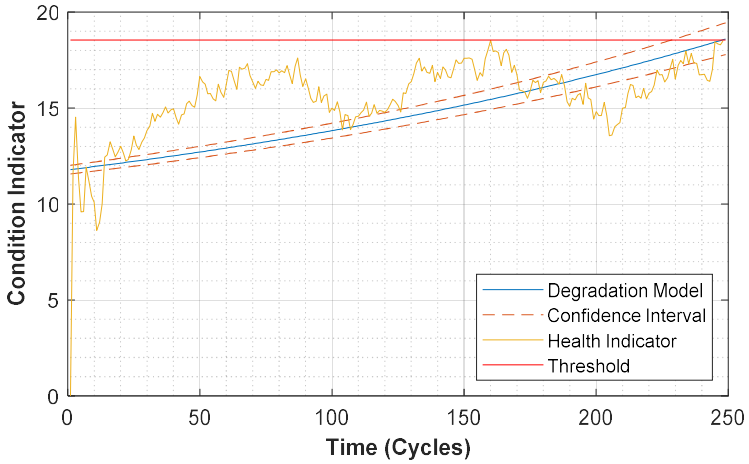

Figure 5.24 (b) Predicted RUL using exponential degradation model Strategy-II

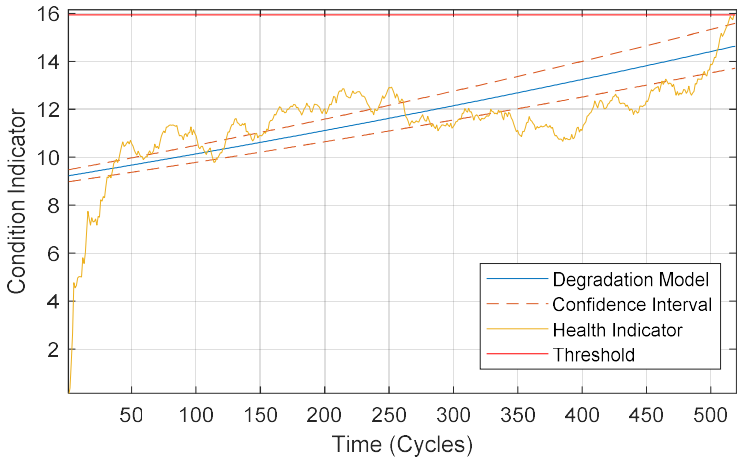

Figure 5.24 (c) Predicted RUL using exponential degradation model Strategy-III

The plots in Fig. 5.24 (a, b, c) reflects the motor RUL predicted over time for 319, 249 and 520 cycles. The data uses exponential degradation model to predict the failure as per the set threshold. Maximum value of the feature fused CI has been the proposed criterion for selecting the threshold. CI's for all three experimental datasets reflect an increasing trend when the motor encounters degradation, and reaches the point of failure. Point of failure is the value where the degradation model meets the final value of the health indicator. Prediction is performed within 95% confidence intervals. Bayesian updating in the process updates the model parameters. A variation in the performance accuracy may be attributed to the presence of the noisy data. The presence of non-Gaussian error has been assumed to be a continuous stochastic process to capture the complexity in the data. Being a time dependent stochastic process, the model parameter, θ and the normal random variable, β is updated to the posterior based on the latest observation of S(t) as reflected in Eq. (11) in Chapter 4 using Bayesian updating.

5.3.3.2 Performance Analysis

In the present study, exponential degradation models are applied to predict the RUL of PMDC motor installed in HIL test setup. Accuracy of the newly developed algorithm based on real time performance is the prime importance to estimate the RUL_T. The condition when RUL_T meets the logged degradation signal, $S(t+t_k) = \ln x_{threshold}$. For a given S(t), the cumulative distribution of RUL_T can be expressed as:

$$F_{RUL_T|S(t)}(t) = p(RUL_T \leq t \mid S_{1:k}) \tag{5.1}$$

The data driven and model based approaches were used for life estimation of metal–oxide–semiconductor field-effect transistor (Celaya et al. 2014). Prediction results using data-driven approach for the PMDC motor dataset depicts the plot between the true value of the RUL (trueRUL) and the estimated value of the RUL (estRUL). Fig. 5.25(a, b, c) shows the accuracy of the results between the true and estimated RUL for 319, 249, and 520 cycles. Superiority in performance for exponential model has been observed during the application study for the wear of mechanical tools (Özel and Karpat 2005), bearings (Li et al. 2015a). Further, the value of error's standard deviation was observed to cause variation of CI as it reaches the threshold. It is worth mentioning that the variation in the performance accuracy of 20% accounts to the noise in the data and mean squared error (MSE), root mean squared error (RMSE) along with error index as in Eqs. (5.1) – (5.3) have been adopted to in order to quantify the accuracy results (Saxena et al. 2008 and Zhao et al. 2009). The choice of the appropriate initial values is reflected in the RUL prediction

plots. The 500 runs correspond to the measure of the error while predicting RUL. RUL is predicted, considering initial degradation starts after 60% of the dataset. Prediction accuracy for the PMDC motor is much higher in case of Strategy-I data than compared to the Strategy-III dataset. However, data from Strategy-II was found to be least accurately predicted. In order to have an estimated design life for a population of motors, this type of lifetime estimating approach may be required during the development or testing stage before the final object comes into use. Users, on the other hand, should be aware that once observable degradation data is available, it is desirable to individually anticipate the RUL in order to make an adaptive decision.

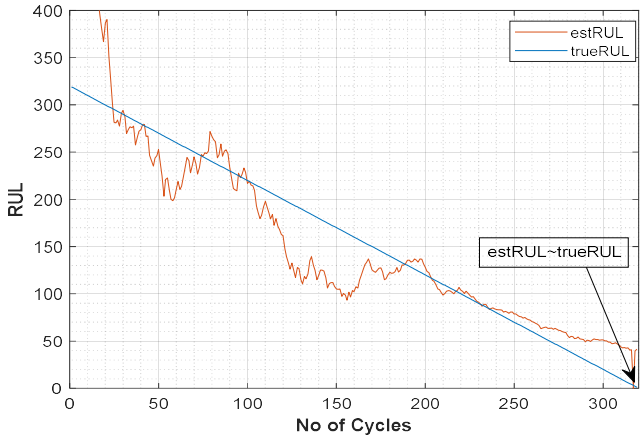

Figure 5.25 (a) Plot of estimated RUL and true RUL for Strategy-I

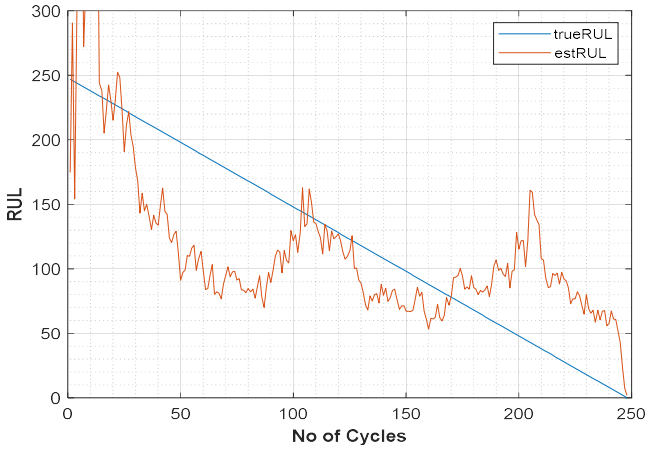

Figure 5.25 (b) Plot of estimated RUL and true RUL for Strategy-II

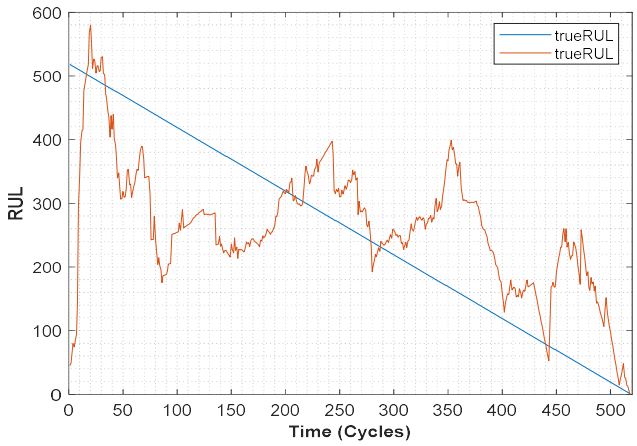

Figure 5.25 (c) Plot of estimated RUL and true RUL for Strategy-III

It is important to note that the criticality in the prediction of failure is higher near the end of life as compared to the beginning. The convergence characteristic of RUL curve towards the end confirms the appropriate selection of the model parameters. The error index (Xu et al. 2014) using Eq. (5.3) was utilized to assess the prediction quality. The Eq. (5.3) follows the general idea of correlation coefficient. All the accuracy metrics can be found tabulated as under Table 5.2.

$$MSE = \frac{1}{N}\sum_{i=1}^{N}(tRUL_i - eRUL_i)^2 \tag{5.2}$$

$$e\_PR = \frac{\sum_{i=1}^{N}(tRUL-\overline{tRUL})(eRUL-\overline{eRUL})}{\sqrt{\sum_{i=1}^{N}(tRUL-\overline{tRU})^2}\sqrt{\sum_{i=1}^{N}(eRUL-\overline{eRUL})^2}} \tag{5.3}$$

$$RMSE = \sqrt{\frac{1}{N}\sum_{i=1}^{N}\left(tRUL_i - eRUL_i\right)^2} \tag{5.4}$$

Table 5.2 Prognostic Accuracy Results

	Strategy I	**Strategy II**	**Strategy III**
***e*_PR**	0.8708	0.6258	0.5755
RMSE	30.2554	78.0280	52.6197
MSE	912.5286	6088.3676	2768.833

Notations, tRUL and eRUL respectively denote true-remaining useful life and estimated-remaining useful life. 0 <e_PR< 1 defines the acceptable range of values. The larger value signifies a better prediction. e_PR has been found to be 0.8708, 0.6258 and 0.5755 for the exponential model in case of three different strategies.

5.3.4 Adaptive filtering

This section presents an on-line particle filtering based framework for failure prognosis in nonlinear, non-Gaussian systems. The advantage of Bayesian formulation in PF precedes it as one of the state-of-the-art tool for filtering problems. The choice of PF is its suitability in finding a best estimate for a non-linear noisy state dynamic. The choice between these filters depends on the dynamics of the system and the shape of the noise distributions. Robust estimates are favorable with the appropriate choice of noise along with the initial parameter values, thus assist in building a fail-safe model. Sub-section 5.4.1 corresponds to CI's obtained from all the three strategies after feature fusion technique. In the subsequent sections, the CI values from the preprocessed technique via stochastic approach will be used for further analysis.

5.3.4.1 Strategy-I: (50%-70%)

It is evident that the motor degrades over cycles in use and the threshold at which the motor fails is the maximum (peak) value in the present dataset. An empirically fitted cubic model is found to fit the degradation data, which has four parameters, namely *p1*, *p2*, *p3,* and *p4*. The parametric function can be used to model the underlying trend.

$$f(t) = p1 * t^3 + p2 * t^2 + p3 * t + p4 \quad (5.4)$$

The randomness in regression parameters has been often assumed to characterize the discrete heterogeneity(Liu and Huang 2016). For large number of applications, the parametric modeling sometimes becomes a challenge because of the presence of irregularity in the underlying trend. The noise in the parameters has been determined from the order of the magnitude of the initial values (Zhang et al. 2018). Table 5.3 presents the parameter values for the fitted model coefficients along with the true noise values.

Table 5.3 Empirically fitted cubic polynomial parameters

Parameters	True value	Upper limit	Lower limit	Noise standard déviation, N(0, σ)
p1	1.573e-06	1.451e-06	1.695e-06	2.440e-08
p2	-0.0007613	-0.0008206	-0.0007021	1.185e-05
p3	0.1064	0.09822	0.1146	1.60e-3
p4	-3.526	-3.828	-3.224	6.04e-2

The initial approach in the present study is to find the robustness of the data to the fitted model. Sensitivity analysis has been conducted with respect to the model parameters to check the model's sensitivity fitted to the dynamic motor current (I_a) data. To check model's uncertainty, random data has been produced and fitted subsequently to each and every coefficients' limiting values. All the individual model parameters showed consistency in the fitted trend, thus helped in achieving a robust model.

A. Particle Filter

The present study predicts the RUL for a known threshold involving a monotonic degradation cubic model. Problem definition includes defining the measurement dataset, the threshold value, the number of particles used, and the respective 95% confidence interval. Initialization of the states has been done using the mean values (see Table 5.3). The number of particles were taken to be 1000, thus representing the system's hypothetical state. Basically, a PF approach consists of three steps namely, the prediction, update, and the resampling. Prediction at the current step uses the model parameters from the previous steps. Updating of the measurement data provides the likelihood (weights, w) and has been done through the assumptions of the normal distribution. Aiming towards computational accuracy and efficiency (Li et al. 2015b), the four traditional resampling techniques have been applied. Resampling eliminates the low weight particles, thereby reducing the unnecessary computation in the probability of the less likelihood region. The training dataset amounting to 60% has been used to update the prediction without updating the model parameters, thereby comparing the predicted results within specified confidence bounds, thus depicting accuracy in the proposed methodology.

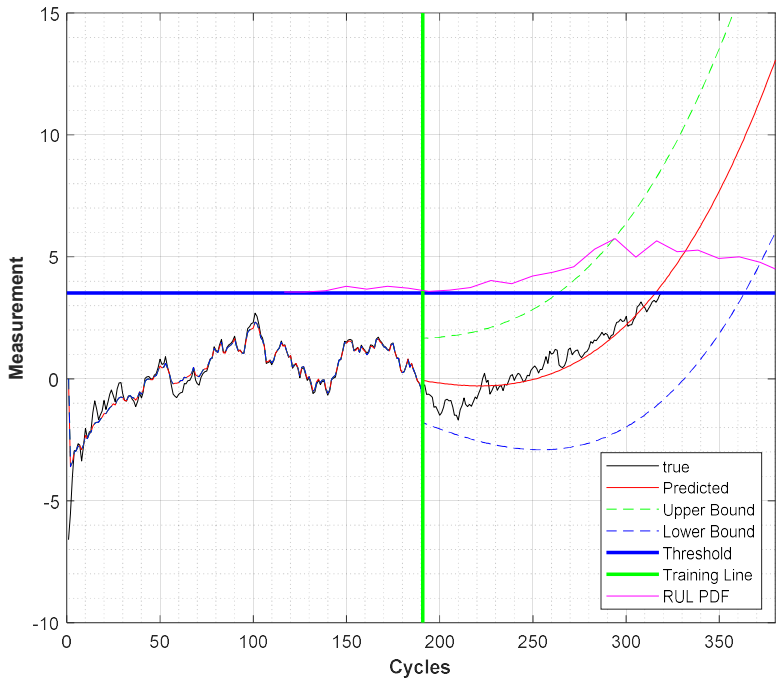

Figure 5.26 State prediction scheme using Particle Filter for Strategy-I

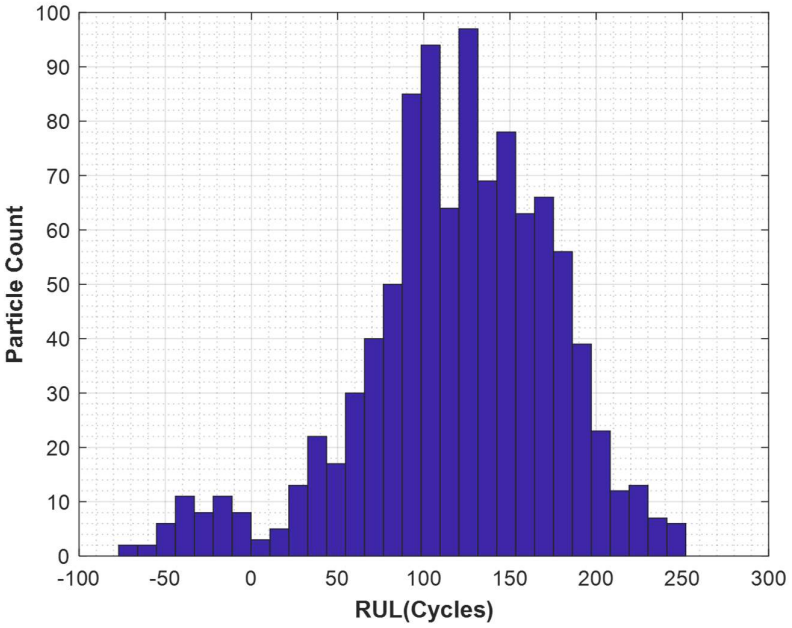

Figure 5.27 Histogram of RUL for Strategy-I

Predicted RUL results (see Fig. 5.26) relating to the PF method demonstrated the proposed approach's underlying performance. Histogram of RUL pdf (see Fig. 5.27) depicted a more significant uncertainty in the bounds of the median value of the predicted RUL (117), which encompasses the need for a much better prediction. The vertical line represented the end of training

data, while the horizontal line represented the failure threshold. Prediction continues till the predicted state reaches the threshold value, i.e., 3.51. Estimated RUL has been obtained by subtracting the current time from the failure time.

B. Unscented Particle Filter

Predicted RUL results (see Fig. 5.28) relates to the UPF method. The use of UT in the approach has been an added smoothness over the traditional PF results. Histogram of RUL pdf in Fig. 5.29 clearly depicts the closeness in uncertainty bounds of the RUL prediction results (134), which proves the basis for the current approach. In Fig. 5.28, the vertical line represents the end of training data, while the horizontal line was the failure threshold. Prediction continues till the predicted state reaches the threshold value (3.51).

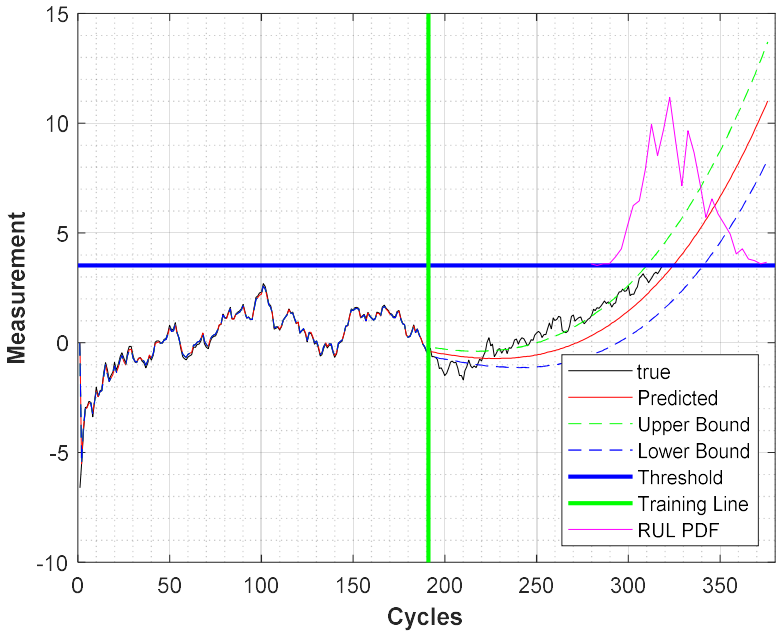

Figure 5.28 State prediction scheme using Unscented Particle Filter for Strategy-I

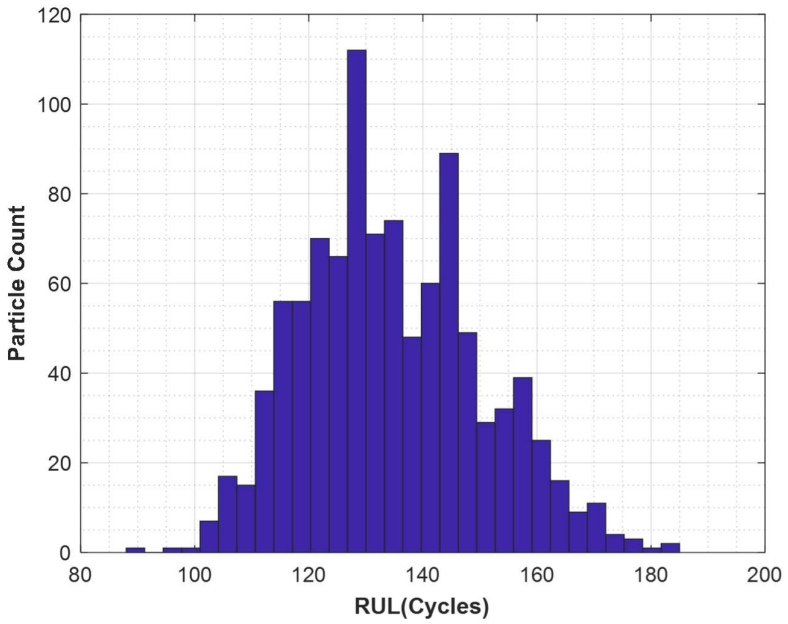

Figure 5.29 Histogram of RUL for Strategy-I

RUL prediction for UPF have been evaluated for 60% of the dataset. Improvement in the RUL pdf has been evident, as shown in the plot of the concise pdf region. The use of the UT scheme for noisy nonlinear data and thereby a substantial increase in the RUL prediction has been evident with the help of UPF. Further accuracy in the RUL prediction results has been observed while implementing the *i*-UPF approach. The *i*-UPF for the present study depends mostly on the optimal choice of *c*-value.

Results and plots along with the table values in the choice of *c*-value and the appropriate resampling shall be found in the subsequent Chapter 6. However, the present chapter will only emphasize upon the PMDC motor RUL estimation results and their effectiveness proposed by the three different PF variants.

C. Improved Unscented Particle Filter

The UT propagates mean and covariance information via nonlinear transformations, in combination with the UKF, as a technique, aids in obtaining a significantly enhanced RUL estimate.

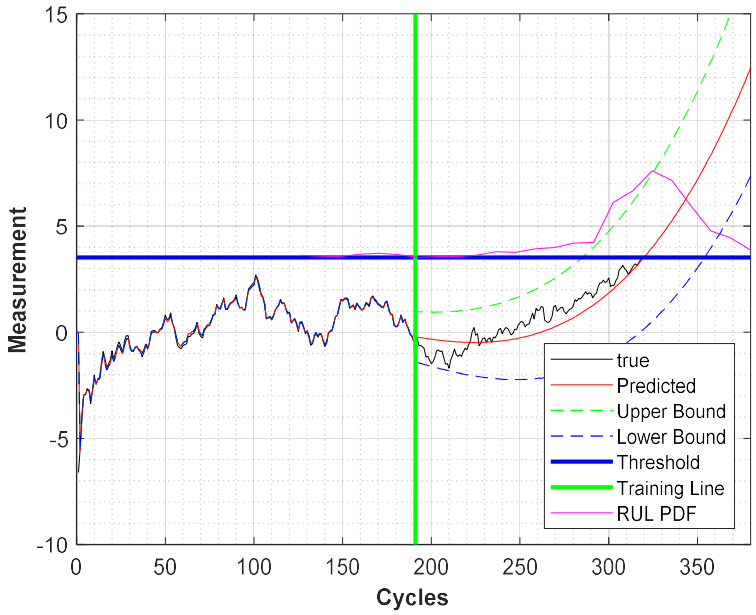

Figure 5.30 State prediction scheme using Improved Unscented Particle Filter for Strategy-I

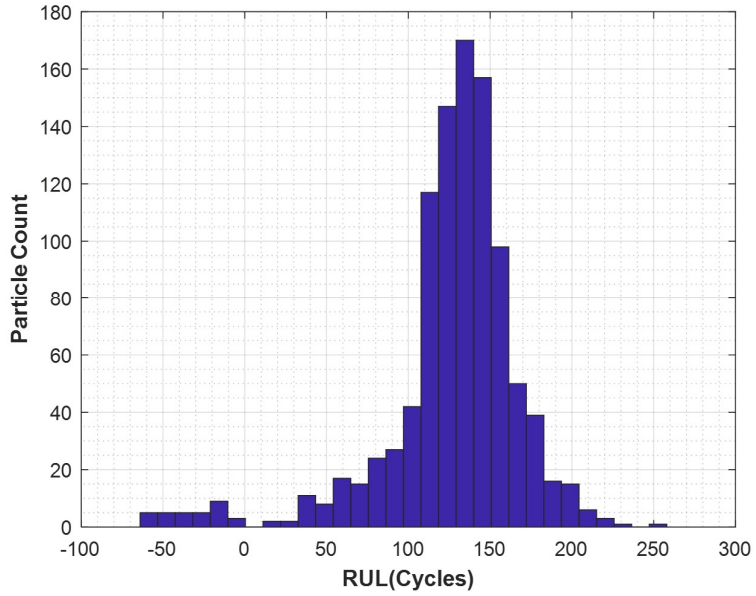

Figure 5.31 Histogram of RUL for Strategy-I

All the results were plotted for a 5% significance level. A much better approximation of the degraded motor and its median value of RUL (131) has been depicted in the converging RUL pdf plots, which has been a measure of effectiveness for the present technique. The peak in the histogram has been evident of reducing uncertainty and increased precision in the results of posterior probability density. Gaussian noise with unknown standard deviation, N(0, σ) has been

used to express the prediction uncertainty. The noise standard deviation has been the covariance of the dataset and values in the range of (0 ~ 2.5) has been tested during computation before finalizing the initial noise values. For a noise value beyond 1.0, there has been no significant difference while predicting the state. Robustness in the RUL prediction results were found, and the *i*-UPF has been the most accurate amongst the three PF methods.

5.3.4.2 Strategy-II: (75%-80%)

The second set consists of a 249cycles data that follows cubic model fitting to the degradation data, by means of four parameters *p1*, *p2*, *p3,* and *p4*. The function form of the model can be found below along with the tabulated model coefficient values, their upper and lower limits and the noise standard deviation chosen for state prediction.

$$f(t) = p1 * t^3 + p2 * t^2 + p3 * t + p4 \quad (5.5)$$

The presence of irregularity in the dataset has been a major reason in selecting the appropriate initial values. The choice of the mutually independent process noise along the parameters has been determined from the order of the magnitude of the initial values. Table 5.4 presents the parameter values for the fitted model coefficients along with the true noise values.

Table 5.4 Empirically fitted parameters

Parameters	True value	Upper limit	Lower limit	Noise standard deviation, N(0, σ)
p1	2.376e-06	2.822e-06	1.93e-06	8.900e-08
p2	-0.000942	-0.0007724	-0.00111	3.396e-05
p3	0.1142	0.1325	0.0959	0.0037
p4	-3.402	-2.873	-3.931	0.106

A. Particle Filter

The sequence of steps while estimating the state and RUL for the motor degradation dataset can be found as discussed in the previous strategy. The problem definition includes the measurement data, failure threshold, the particles used, weights, noise and the respective 95% confidence interval. All the above entities constitute PF as a whole in the state prediction scheme. The true value in Table 5.4 initialize the states vary applies defining val. The 1000particles have been considered representing the system's hypothetical state. For a three steps scheme, the PF along

with the Bayesian approach has been utilized here to estimate the model parameters for the empirically fitted cubic model by means of the prediction, update, and the resampling steps. Prognostics attempts in using the posterior probability density of the estimated model parameters that effects the model behavior. Unlike the Kalman filter that uses Gaussian noise (Shariati et al. 2019), the present work precedes using non-Gaussian for the chosen nonlinear model. Training dataset amounting to 60% has been used to update the prediction and the accuracy results are plotted within specified confidence bounds.

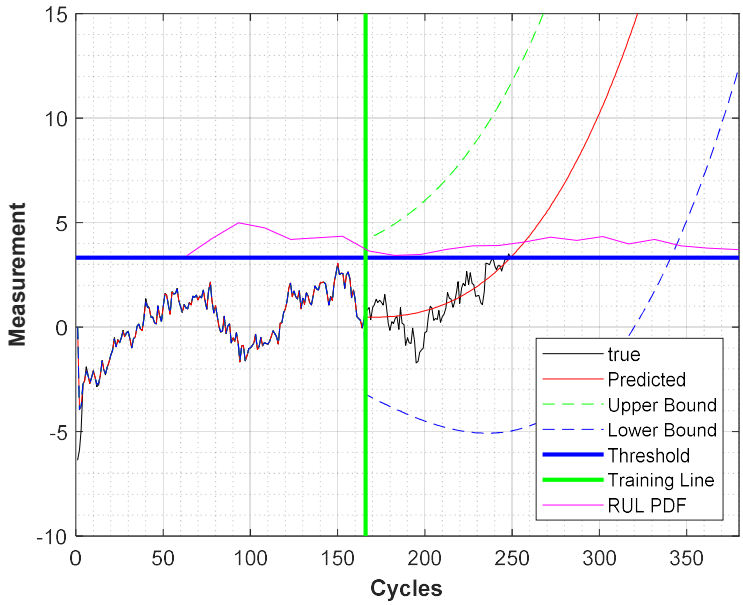

Figure 5.32 State prediction scheme using Particle Filter for Strategy-II

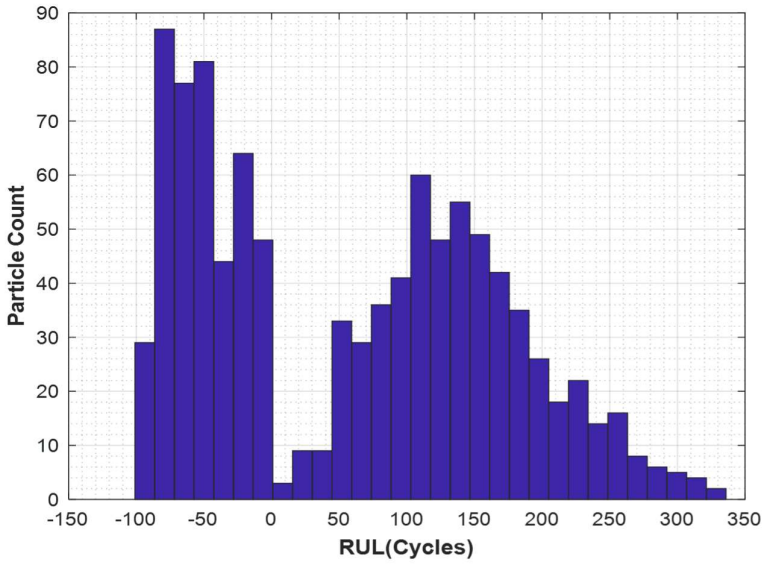

Figure 5.33 Histogram of RUL for Strategy-II

The prediction line in Fig. 5.32 can be found to capture the exact failure point which provides a basis for the selection of the initial choice of the model parameters. The choice of measurement noise also resulted in a very accurate fitting within the confidence bounds. Tests for 500 runs with the multinomial resampling yielded in the robust RUL (79) results.

Histogram of RUL pdf (see Fig. 5.33) proves two peaks due to the closeness of the actual data towards the failure line but towards the end it depicted a more significant uncertainty. encompasses the need for a much better prediction. The vertical line represented the end of training data, while the horizontal line represented the failure threshold. Prediction continues till the predicted state reaches the threshold value, i.e., 3.5056. True RUL has been obtained by subtracting the current time from the failure time.

B. Unscented Particle Filter

The state prediction (see Fig. 5.34) relates to the UPF method. The UPF methodology added accuracy in the results over the traditional PF method. The smoother histogram with a single peak in Fig. 5.35 clearly depicts the decreasing uncertainty while calculating the RUL pdf with median value approaching 83. Prediction continues till the predicted state reaches the threshold value.

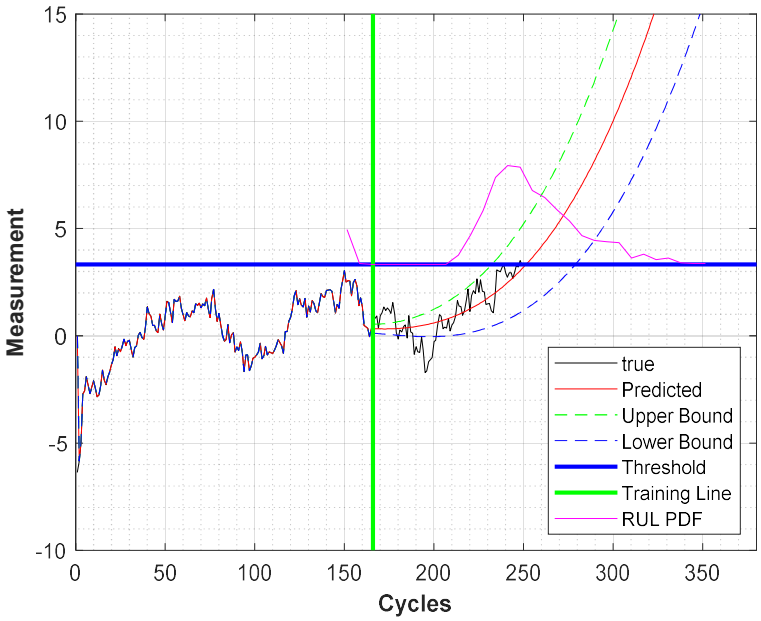

Figure 5.34 State prediction scheme using Unscented Particle Filter for Strategy-II

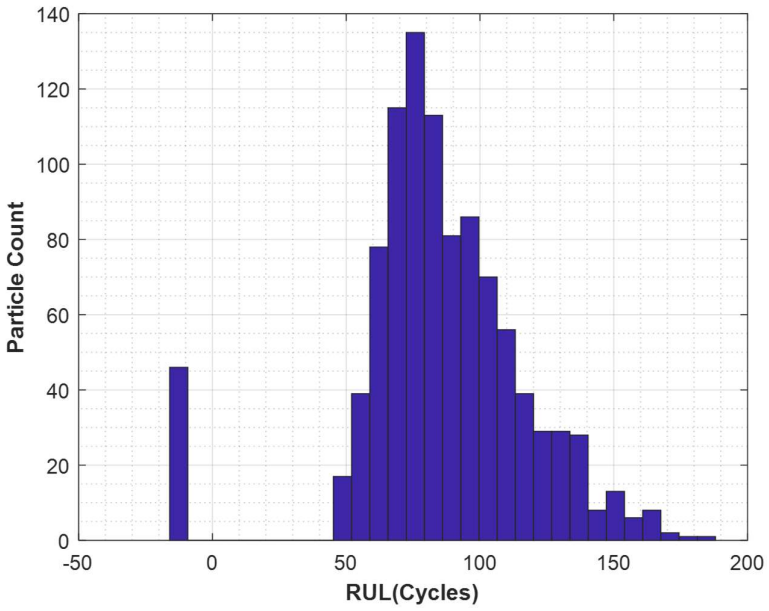

Figure 5.35 Histogram of RUL for Strategy-II

Results of the RUL prediction were evaluated for 60% of the dataset. Improvement in the RUL pdf has been evident, as shown in the pdf plot. Further accuracy in the RUL prediction results has been aimed by using the *i*-UPF approach.

C. Improved Unscented Particle Filter

Results of RUL pdf were plotted for a 5% significance level. A much better approximation of RUL for the degraded motor is reflected by its median value of RUL (84) and the converging RUL pdf plots, which optimizes the uncertainty. The peak in the histogram manifests the decreasing uncertainty and the increased precision in the results of RUL. Gaussian noise, N(0, σ) has been used to express the prediction uncertainty. The noise standard deviation has been the covariance of the dataset and values in the range of (0 ~ 1) has been tested during computation before finalizing the initial noise. For a noise value beyond 0.2, there has been no significant difference while predicting the state. The CI for the aforementioned motor degradation model in Strategy II shows the presence of non-monotonic behaviour which accounts to the second peak of the RUL pdf.

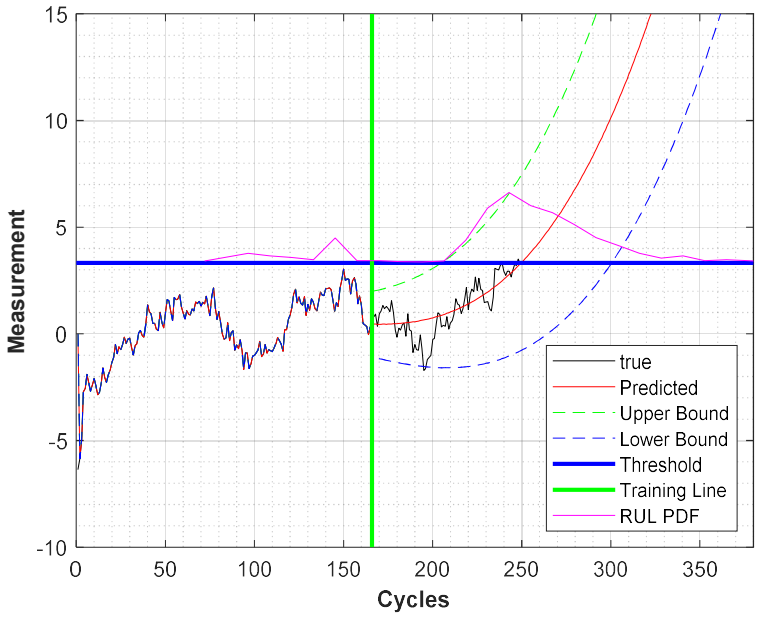

Figure 5.36 State prediction scheme using Improved Unscented Particle Filter for Strategy-II

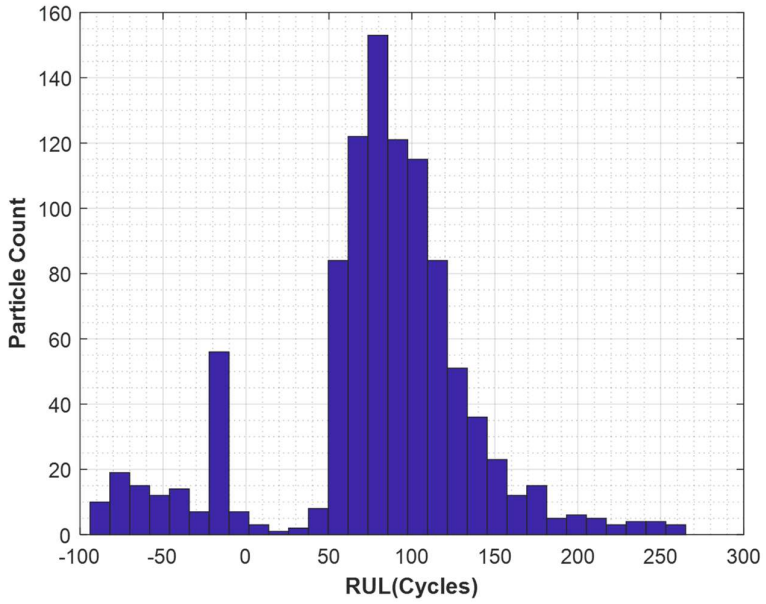

Figure 5.37 Histogram of RUL for Strategy-II

The methodology works well for a monotonic function however limits the use under the changing behavior of the model. Robustness in the RUL prediction results were found, and the *i*-UPF has been the most accurate amongst the three PF methods.

5.3.4.3 Strategy-III: (80%-85%)

The present Strategy III operates under higher PWM that accounts to a reduced operating cycle time. The completion of once cycle time is about 1.05seconds as compared to the earlier instances which encountered 1.06 and 1.09 seconds for Strategy I and Strategy II respectively. A four parameter cubic model provides the goodness-of-fit to the degradation motor data and is expressed in Eq. (5.6).

$$f(\mathrm{t}) = p1*\mathrm{t}^3 + p2*\mathrm{t}^2 + p3*\mathrm{t} + p4 \qquad (5.6)$$

Table 5.5 presents the parameter values for the fitted model coefficients along with the true noise values.

Table 5.5 Empirically fitted parameters

Parameters	True value	Upper limit	Lower limit	Noise standard deviation, N(0, σ)
p1	3.866e-07	4.113e-07	3.62e-07	4.930e-09
p2	-0.0003229	-0.0003033	-0.0003424	3.910e-06
p3	0.08196	0.08635	0.07757	0.00088
p4	-5.791	-5.527	-6.055	0.053

The consistency in trend has been observed for the data, that assists in achieving a robust model. The use of dynamic motor current (I_a) data depicts the presence nonlinearity and the covariates of the data indicates the presence of non-Gaussian noise. The coefficients' limiting values assists in proper selection of the initialization of the model thereby helps in achieving less uncertain results.

A. Particle Filter

The monotonic degradation model in the present section has been used to present the state prediction scheme. RUL prediction is done using extrapolation method and a known failure threshold. PF being a sequential Monte Carlo approach, takes into account the measurement dataset, failure threshold value, number of particles, and predicts within 95% confidence interval. Initialization of the states has been done using the values offered in Table 5.5. Results were produce with 1000 particles. Bayesian updating follows the PF state prediction scheme that uses the particles as the ones having information for the unknown state parameters. Probability density functions are generated for the unknown observations with the help of the current observations

and an update scheme. The PF can be better stated as a "*prediction by state and correction by measurement*". The training data amounting to 60% has been used to update the prediction without updating the model parameters, thereby comparing the predicted results within specified bounds that depicts accuracy of the proposed scheme.

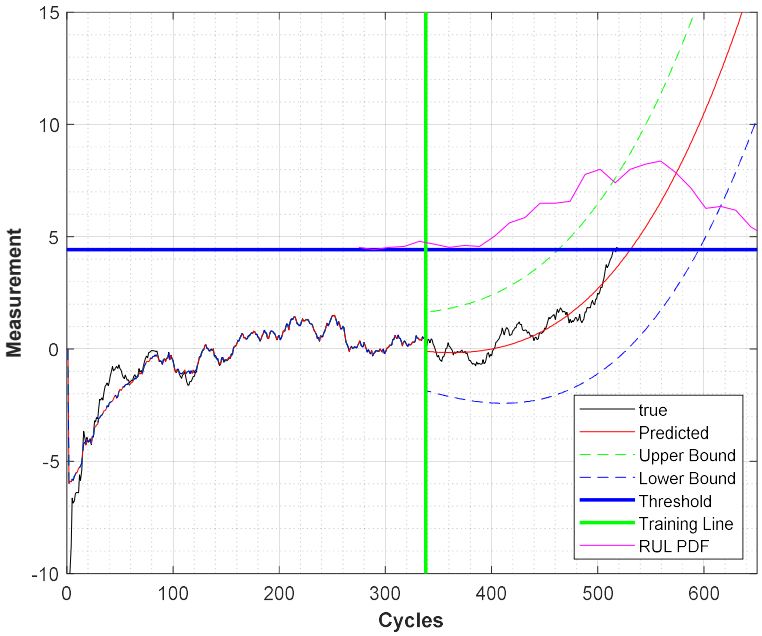

Figure 5.38 State prediction scheme using Particle Filter for Strategy-III

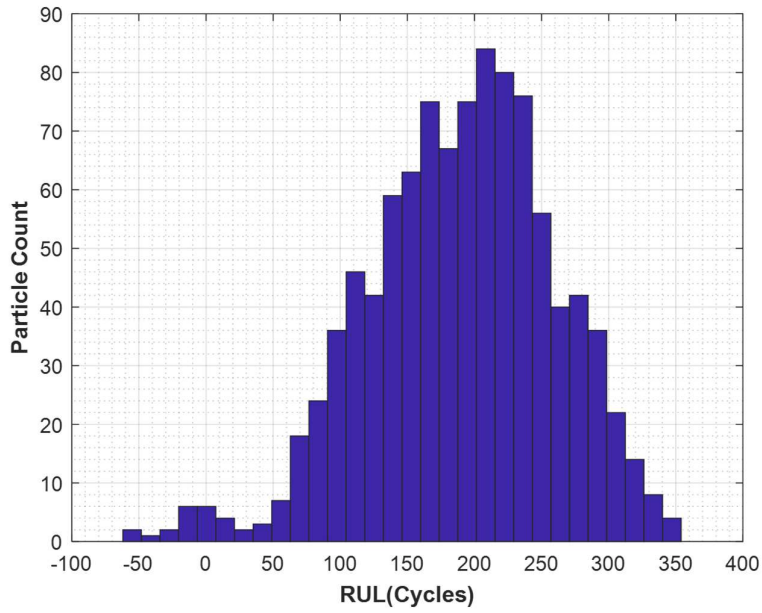

Figure 5.39 Histogram of RUL for Strategy-III

Tests for 500 runs have been performed where multinomial resampling proved to be the best for *i*-UPF, UPF and PF techniques. However, further discussion about the precision level of multinomial resampling in context to RUL prediction error will be discussed in the next chapter.

State prediction within confidence bounds in Fig. 5.38 demonstrates the efficiency using PF method. Histogram of RUL pdf (see Fig. 5.39) illustrate the uncertainty in the bounds of the predicted RUL (214), which encompasses the need for a much better prediction. As compared to other datasets, the strategy III resembles highly monotonic. Prediction continues till the state value encounters a failure threshold, i.e., 4.51. True RUL has been obtained by subtracting the current time from the failure time.

B. Unscented Particle Filter

The UPF predicted RUL results in Fig. 5.40 shows an improved RUL pdf plot with a confined peakedness. The use of nonlinear transform for a set of data sample has provided an additional value over the traditional PF results. The vertical line and the horizontal line represents the end of training data, and the failure threshold respectively.

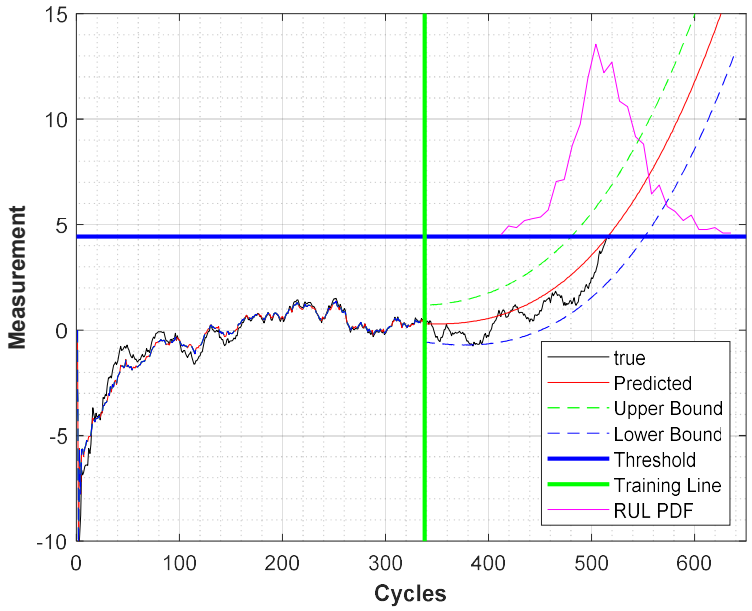

Figure 5.40 State prediction scheme using Unscented Particle Filter for Strategy-III

For the initial part of the noisy data, the state prediction finds difficult to closely relate to the true dataset. However, the 60% amount of training data results in obtaining a peaked RUL pdf. Improvement in the RUL pdf has been evident, as shown in the plot of the pdf concise area. The use of the UT scheme for noisy nonlinear data and thereby a substantial increase in the RUL

prediction has been evident with the help of UPF. Uncertainty in the RUL prediction is found to be very less as depicted from its median value (205) of RUL prediction, which proves the basis for the current approach.

Further improvement in the RUL pdf results is aimed by means of using the *i*-UPF approach.

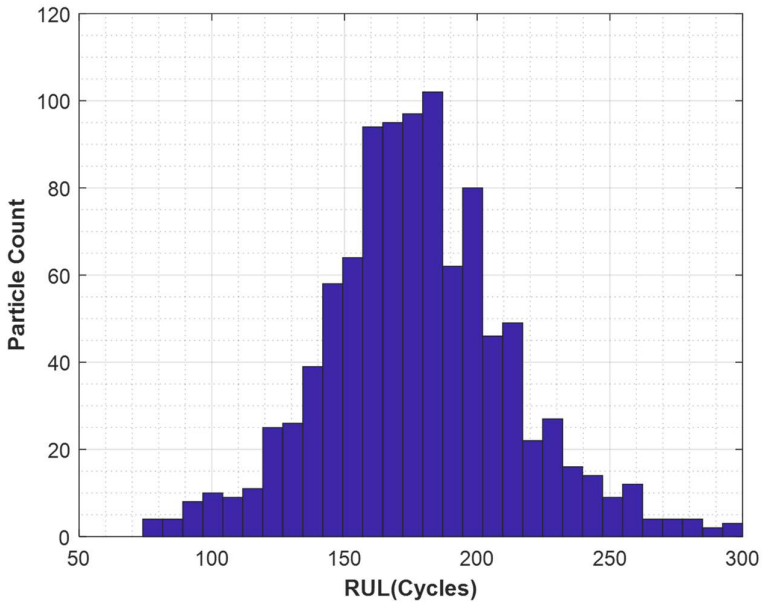

Figure 5.41 Histogram of RUL for Strategy-III

C. Improved Unscented Particle Filter

The *i*-UPF worked on developing a novel sample processing approach with the goal of improving predictability. To pick and change particle samples, the new technique presents a desired region. It accepts all expected samples that are already in the region and concentrates the rest of the samples that aren't in the interval between the remote and high likelihood regions of the probability density function. Comparison of the state predictions with the three PF variants shows the superiority of the posterior pdf.

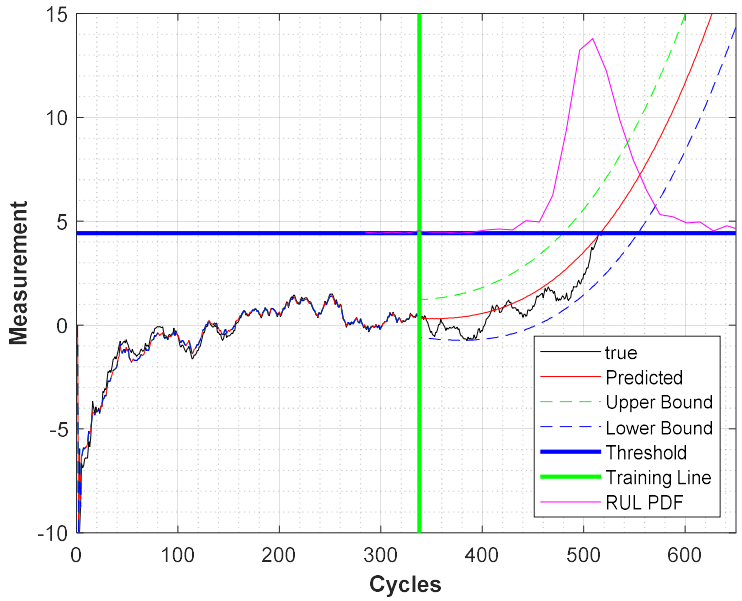

Figure 5.42 State prediction scheme using Improved Unscented Particle Filter for Strategy-III

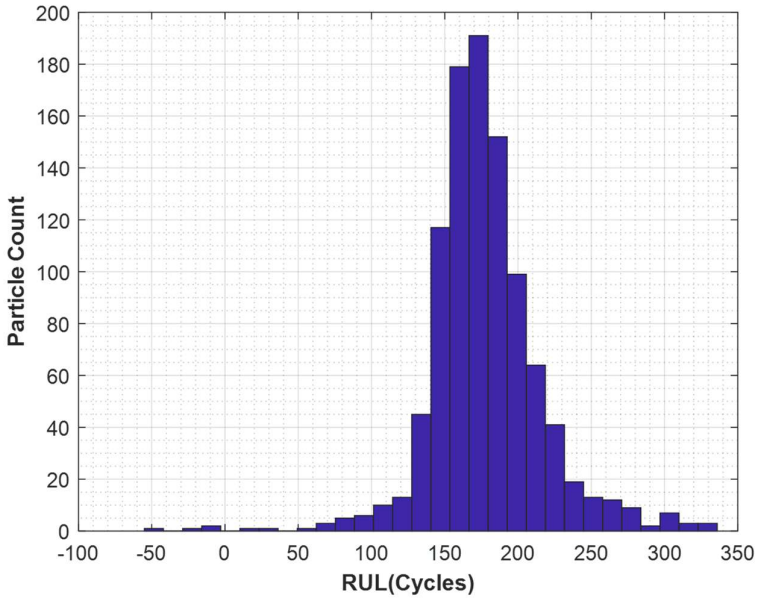

Figure 5.43 Histogram of RUL for Strategy-III

All the computations were performed for 500 runs and a 5% significance level. A much better approximation of the RUL pdf for the degraded motor using 1000particles has been depicted in the converging RUL pdf plots and the histogram, which has been a measure of decreasing uncertainty. The histogram has a closer resemblance to that of the normal distribution, which is evident of reducing uncertainty and increased precision in the results of RUL (207). The noise standard deviation has been the covariance of the dataset and values in the range of (0 ~ 2) has

been tested during computation before finalizing the initial noise. For a noise value beyond 1.0, there has been no significant difference while predicting the state. Lesser magnitude of the noise value showed an abrupt histogram with imperfect prediction. Repeated computation results for RUL prediction proved the robustness of the proposed scheme and the *i*-UPF has been the found to be most accurate amongst the three PF variants.

5.3.5 Comparison of Prognostic Accuracy Results

The results aim towards comparison of the superior technique in order to find an accurate motor RUL. It has been important to note that for the ALCT data, the criticality in predicting failure has been observed towards the end as compared to the beginning. Due to the presence of an ample length of data points in all the three strategies, the parameter update has been found to be smoother. Starting from the beginning until the point of training i.e., 60% of the dataset, state prediction is found to be very smooth. Exhaustive computation has been conducted and accuracy results were found for all the respective number of cycles. The maximum value of the dataset has been the pre-set failure point or the threshold in the dataset. Present scope of the work deals with Type III prognostics, that uses a known failure threshold to evaluate the RUL. The fulfillment of the primary aims, i.e., the accuracy, robustness and ease of computational complexity, has been achieved. A larger number of particles has been aimed towards accuracy, while a lesser number of particles has helped in achieving the computational benefits. Experiments were conducted using different particle sets and finally a set of 1000 particles has provided moderately improved benefits.

The correctness has been further evaluated from the derived accuracy metrics. The well-known measures (Jouin et al. 2016) such as the RMSE, MSE and the error index (e_PR) have been chosen for estimating the statistical significance of predicted RUL results. Their expressions can be found in Eqs. (5.3) – (5.6) while the measures can be found documented in Table 5.6.

Table 5.6 Comparison of prognostic accuracy results for Strategy-I dataset

Strategy-I				
	Particle Filter	Unscented Particle Filter	Improved Unscented Particle Filter	Exponential Degradation Model
*e*_PR	0.9135	0.9325	0.9421	0.8708
RMSE	0.0273	0.0271	0.0257	30.2554
MSE	0.0135	0.0175	0.0165	912.5286

Computation for accuracy were further extended for another 249cycles and 520cycles dataset respectively. The respective cycle values are the failure points during experimentation. For a known threshold and favoured initial conditions along with noise standard deviations, the accuracy in the RUL prediction was seen to fairly increase. The value of error index was seen to decrease in the case of Strategy-II as compared to Strategy-I dataset, while the other metrics had consistency in accuracy. For an exponential degradation model, the error index yielded superior results as compared to RMSE and MSE. The values itself clearly indicated that adaptive filtering techniques outperformed the stochastic approach in case of Strategy-I dataset.

Table 5.7 Comparison of prognostic accuracy results for Strategy-II dataset

Strategy-II				
	Particle Filter	Unscented Particle Filter	Improved Unscented Particle Filter	Exponential Degradation Model
*e*_PR	0.9051	0.9381	0.9499	0.6258
RMSE	0.0132	0.0195	0.0175	78.0280
MSE	0.0328	0.0224	0.0219	6088.3676

Table 5.7 illustrates a robust and accurate RUL estimation while utilizing adaptive filtering upon Strategy-II dataset. For a 60percent training dataset, the model coefficients were updated, while beyond the training line the prediction was performed using the past set of tuned model parametric values. Exhaustive computation with 1000 particles and for 500 runs were extended for obtaining highly improve results. Taking into account all three strategies, the *i*-UPF approach was able to overcome sample impoverishment (Zhang et al. 2018), resulting in a very efficient process for properly predicting RUL. Consistent results (see Table 5.8) of the adaptive filtering techniques were seen to outperform the exponential degradation modelling for all the experimental strategies.

Table 5.8 Comparison of prognostic accuracy results for Strategy-III dataset

Strategy-III				
	Particle Filter	Unscented Particle Filter	Improved Unscented Particle Filter	Exponential Degradation Model
*e*_PR	0.9438	0.9490	0.9498	0.5755
RMSE	0.0492	0.0336	0.0322	52.6197
MSE	0.0086	0.0126	0.0192	2768.833

5.4 Summary

This study helps to understand the merit and demerit of the two data-driven degradation models for a nonlinear noisy dataset operating under harsh conditions. Exponential degradation modelling and Adaptive filtering have been adopted for evaluating the RUL of the clutch motor system operating under accelerated loading conditions. Initially, the approach to data handling and appropriate selection of the CI has been featured. With the finalized CI's from all the three experimental strategies exponential degradation modeling was attempted and RUL by means of extrapolation was computed within a maximum achievable accuracy. The exponential degradation model demonstrates the effectiveness in reducing the effect of random errors of the stochastic process while compromising the desirable accuracy in RUL estimation. Subsequently, three variants of PF a.k.a., PF, UPF and *i*-UPF have been used aiming towards improving the efficacy towards RUL estimation. Comparison of the RUL accuracy clearly demonstrated the dominance of the adaptive filtering techniques when applied upon all the three experimental datasets. The *i*-UPF has been most efficient in state prediction while the proposed adaptive approach provided a robust estimate.

Also with resampling coming into effect, how each of the four techniques has an effect on computational time besides accuracy needs to be addressed. The choice of *i*-UPF depends on the appropriate *c*-value which needs further discussion. Results indicate that there is a scope of further study with clarification as to which variant of particle filtering can obtain highly improved RUL results.